

Review

Open Access



High entropy photocatalysts for energy and environmental applications

Liquan Jing^{*} , Hui Wang, Tayebbeh Roostaei, Amir Varamesh, Qi Gao, Jinguang Hu^{*}

Department of Chemical and Petroleum Engineering, University of Calgary, Calgary T2N1N4, Alberta, Canada.

^{*}**Correspondence to:** Dr. Liquan Jing; Prof. Jinguang Hu, Department of Chemical and Petroleum Engineering, University of Calgary, 2500 University Drive, NW, Calgary T2N1N4, Alberta, Canada. E-mail: liquan.jing@ucalgary.ca; jinguang.hu@ucalgary.ca

How to cite this article: Jing, L.; Wang, H.; Roostaei, T.; Varamesh, A.; Gao, Q.; Hu, J. High entropy photocatalysts for energy and environmental applications. *Chem. Synth.* **2025**, *5*, 36. <https://dx.doi.org/10.20517/cs.2024.52>

Received: 16 Apr 2024 **First Decision:** 14 Jun 2024 **Revised:** 8 Jul 2024 **Accepted:** 16 Jul 2024 **Published:** 18 Mar 2025

Academic Editor: Jin Xie **Copy Editor:** Pei-Yun Wang **Production Editor:** Pei-Yun Wang

Abstract

Today, the energy and environmental crisis originating from the use of fossil fuels and carbon dioxide (CO₂) emissions has become a common concern in lives of people. Photocatalysis is a promising clean technology receiving much attention. There are diverse strategies to enhance the efficiency of photocatalysis, and high entropy photocatalysts (HEPs) show great potential as new efficient photocatalysts. The tunability of HEPs provides more possibilities for the design of the electronic structure of the catalysts, which leads to the efficient separation of electron-hole pairs and substantially enhances the photocatalytic performance. This review discusses the composition of HEPs, their advantages in photocatalysis, characterization, and prediction, and the latest applications of various photocatalytic systems. Finally, we discuss and summarize the challenges and the prospects of HEPs.

Keywords: Design, high-entropy, photocatalysis, energy, environment

INTRODUCTION

Photocatalysis is a process that utilizes light energy to initiate a chemical reaction on the surface of a catalyst, which has several advantages in the energy and environmental fields^[1-8]. It utilizes sunlight as the primary energy source for sustainable and renewable energy conversion processes. By converting solar energy into chemical energy, photocatalysis contributes to the development of solar-powered fuel



© The Author(s) 2025. **Open Access** This article is licensed under a Creative Commons Attribution 4.0 International License (<https://creativecommons.org/licenses/by/4.0/>), which permits unrestricted use, sharing, adaptation, distribution and reproduction in any medium or format, for any purpose, even commercially, as long as you give appropriate credit to the original author(s) and the source, provide a link to the Creative Commons license, and indicate if changes were made.



production and energy storage technologies^[9-12]. Photocatalytic processes typically take place under mild conditions, requiring only light and a catalyst, without additional chemicals or high temperatures. They provide a green and sustainable approach to energy production and environmental remediation, minimizing environmental impact and waste generation^[13-18]. Overall, photocatalysis holds great promise for addressing energy and environmental challenges through the utilization of renewable energy sources, the promotion of clean energy technologies and the mitigation of pollution and climate change impacts^[19-25]. Continued research and technological advances in the field of photocatalysis continue to expand its applications and increase its efficiency and effectiveness in various fields.

The core of photocatalytic technology is the design of photocatalysts. High entropy photocatalysts (HEPs) are a new class of materials that have recently attracted great attention in the field of materials science and chemistry. High entropy varies in definition in different fields. In thermodynamics, entropy is a physical quantity that measures the degree of chaos of a system; the larger the entropy value, the more uniform the energy distribution, the more chaotic the system is, and the system is in the most chaotic state when maximum entropy is reached. In materials science, high-entropy materials are a specially designed material concept characterized by multimodal mixing, equimolar or nearly equimolar ratios, increased entropy, complex crystal structures, and multifunctionality. These materials are composed of five or more different elements with atomic percentages of each element ranging from 5% to 35%, forming a homogeneous solid solution structure with high mixing entropy and disordered atomic arrangements leading to new physicochemical properties. Both embody the properties or states of a system in a state of high entropy, although in different domains^[26-28]. Non-HEPs consist of single or few elements, resulting in simpler structures that are easier to understand and characterize. However, their performance in complex catalytic reactions may not match that of HEPs. These non-HEPs typically have a singular function and lack the flexibility of high-entropy materials^[29]. Unlike conventional non-HEPs, HEPs comprise five or more major elements in close to iso-atomic proportions^[30-33]. This unique composition results in a rich variety of crystal structures and properties. The different elemental compositions of HEPs can produce unique electronic structures that enhance light absorption, charge separation, and the overall efficiency of the photocatalytic process^[31,34,35]. In addition, high conformational entropy contributes to the stability and durability of photocatalysts under operating conditions. This is particularly important for practical applications where long-term performance is critical. In summary, HEPs represent an exciting frontier in materials science, providing new paradigms for the design of materials with tailored properties suitable for advanced photocatalytic applications. The synergistic effects generated by multiple major elements in these materials offer the possibility of achieving higher efficiency and stability than conventional photocatalysts. As research in this area continues to evolve, it promises to make a significant contribution to sustainable energy solutions and environmental protection efforts.

This review firstly discusses the elemental composition region and range of HEPs, various synthesis strategies of HEPs (focusing on high-temperature calcination), the advantages of HEPs in photocatalysis (adjustability, broad spectrum absorption, enhanced photocatalytic performance, customizability, high stability), multiple structural/optical characterizations and theoretical calculations of HEPs, prediction of HEPs by machine learning (ML), applications and distribution of HEPs in photocatalysis (e.g., degradation, hydrogen (H₂)/oxygen (O₂) production, CO₂ reduction, biomass conversion, organic conversion, *etc.*) were analyzed [Figure 1]. Finally, the challenges and application prospects of HEPs are envisioned.

THE COMPOSITION OF HEPS

The concept of high-entropy materials, including high-entropy photocatalytic materials, is based on the idea of mixing multiple elements in approximately equimolar ratios to create materials with unique properties.

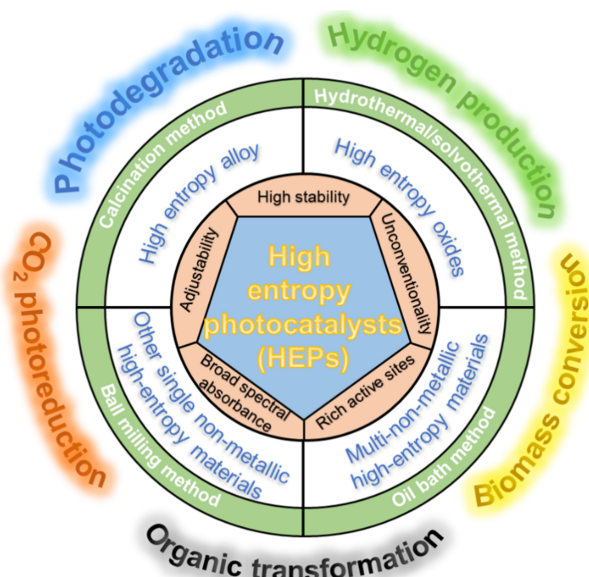


Figure 1. Schematic diagram of all relevant contents of HEPs. HEPs: High entropy photocatalysts.

Although there are no strict rules for the constituent elements of high-entropy photocatalytic materials, some principles and guidelines have been proposed to guide their design and synthesis^[26,30,35,36]. The following are some considerations:

- (a) Elemental diversity: High-entropy photocatalytic materials should contain a variety of elements to enhance their complexity and performance. The inclusion of multiple elements can lead to a high degree of disorder in the material, which can promote synergistic effects and improve photocatalytic performance.
- (b) Similar electronegativity: The constituent elements should have similar electronegativity to avoid the formation of segregation or phases within the material. This promotes the formation of single-phase solid solutions with a uniform distribution of elements.
- (c) Thermodynamic stability: The selected elements should form stable compounds or solid solutions to ensure the stability of the high-entropy material. Thermodynamic calculations and phase diagrams can help predict the stability of multi-component systems.
- (d) Compositional balance: Although equimolar ratios are commonly used in high-entropy materials, the exact composition may vary depending on the specific application and desired properties. Composition can be adjusted to optimize photocatalytic activity, band gap, electronic structure, and other relevant parameters.
- (e) Tailored properties: The compositional elements should be selected to impart the desired properties of the photocatalysis, such as suitable band gap, band edge positions, surface reactivity and carrier dynamics. This may involve the selection of elements with appropriate electronic configurations and orbital hybridization.
- (f) Synergistic effects: The combination of multiple elements in a high-entropy photocatalytic material can produce synergistic effects that enhance the properties of the material compared to a single component or a binary alloy. These synergistic effects may arise from interactions between different elements, electronic effects, or structural effects.
- (g) Experimental validation: The design of high-entropy photocatalytic materials should be complemented by experimental characterization and testing to assess their performance. This may involve the assessment of photocatalytic activity, stability, surface reactivity, charge transfer kinetics and other relevant properties.

Overall, the design of high-entropy photocatalytic materials involves a balance of thermodynamic considerations, material properties, and desired functionality. As research in this area continues to progress, new strategies and guidelines for designing high-entropy materials with tailored photocatalytic properties may emerge. From [Figure 2](#), we can find that the most used metallic elements at present are mainly focused on transition metals (among which Mn, Fe, Co, Ni, and Cu are most frequently used), and the nonmetals are mainly a few main-group elements (N, O, P, and S), which have been widely used and also provide some guidance for the preparation of our HEPs.

SYNTHETIC STRATEGIES FOR HEPs

The mainstream types of HEPs include: high entropy oxides, high entropy sulfides, high entropy alloys, high entropy phosphides, high entropy nitrides, high entropy oxynitrides, and high entropy metal-organic frameworks (MOFs). These HEPs were synthesized by various methods, among which high temperature calcination is still the main synthesis strategy [[Figure 3](#)]. This is mainly due to some special advantages that can be possessed at high temperatures: (1) phase stability (High temperature calcination promotes the formation of stable crystalline phases in high-entropy materials, which ensures structural integrity and resistance to phase change during the photocatalytic reaction. This stability enhances the long-term performance and durability of the photocatalyst); (2) homogeneous mixing (High temperature calcination facilitates the diffusion and mixing of multiple elements, leading to a uniform distribution of components within the material. This homogeneous mixing promotes synergistic interactions between the elements, maximizing the effectiveness of the high-entropy compositions); (3) crystal growth and morphology control (High temperature calcination controls crystal growth and morphology development in high-entropy photocatalytic materials. This enables the regulation of particle size, shape, and surface properties, which significantly affects photocatalytic activity and efficiency); (4) enhanced photocatalytic activity (High temperature treatment during calcination can induce structural changes and defect formation in the material, thereby enhancing its photocatalytic activity. These changes can improve light absorption, charge separation and surface reactivity, thus enhancing photocatalytic performance); (5) optimized energy band structure (High temperature calcination can affect the electronic energy band structure of high-entropy materials, resulting in the formation of energy levels suitable for photocatalytic processes. This optimization of the energy band structure enhances the ability of the material to effectively utilize light energy for catalytic reactions); (6) reducing surface contamination (High temperature calcination removes surface contaminants and impurities from the material, resulting in a cleaner surface and improved photocatalytic performance. This process helps to enhance the surface reactivity of the material and minimize unwanted side reactions); (7) scalability and reproducibility (High temperature calcination methods are often scalable and reproducible, making them suitable for large-scale production of high-entropy photocatalytic materials. This enables the synthesis of materials with consistent properties and performance, facilitating their practical application in a variety of photocatalytic systems); and (8) compatibility with a wide range of compositions (High temperature calcination can be applied to a wide range of compositions and precursor materials, allowing it to be used to synthesize different types of HEPs. This flexibility allows researchers to tailor material properties to meet specific photocatalytic requirements). Overall, high temperature calcination provides a robust and effective method to synthesize high-entropy photocatalytic materials with enhanced structural, morphological, and electronic properties, resulting in improved photocatalytic activity and efficiency. Furthermore, this method is crucial for synthesizing HEPs. This process typically involves temperatures ranging from 600 to 1,200 °C, and the calcination duration can vary from a few hours to several dozen hours, depending on the material's complexity. The selection of calcination conditions must meet the catalyst's application requirements, considering factors such as thermal stability, crystal structure, and targeted photocatalytic performance. Therefore, determining the appropriate calcination temperature and time is an essential step in the synthesis of HEPs. In addition to the synthesis strategies mentioned

IA																	0									
H	II A	Most metal elements used				Other metal elements used				Non-metallic elements used				III A	IV A	V A	VIA	VII A	He							
Li	Be																				B	C	N	O	F	Ne
Na	Mg	III B	IV B	V B	VI B	VII B	VIII B				I B	II B	Al	Si	P	S	Cl	Ar								
K	Ca	Sc	Ti	V	Cr	Mn	Fe	Co	Ni	Cu	Zn	Ga	Ge	As	Se	Br	Kr									
Rb	Sr	Y	Zr	Nb	Mo	Tc	Ru	Rh	Pd	Ag	Cd	In	Sn	Sb	Te	I	Xe									
Cs	Ba	La-Lu	Hf	Ta	W	Re	Os	Ir	Pt	Au	Hg	Tl	Pb	Bi	Po	At	Rn									
Fr	Ra	Ac-Lr	Rf	Db	Sg	Bh	Hs	Mt	Ds	Rg	Cn	Uut	Fl	Uup	Lv	Uus	Uuo									

La	Ce	Pr	Nd	Pm	Sm	Eu	Gd	Tb	Dy	Ho	Er	Tm	Yb
Ac	Th	Pa	U	Np	Pu	Am	Cm	Bk	Cf	Es	Fm	Md	Mo

Figure 2. Commonly used elements in HEPs. HEPs: High entropy photocatalysts.

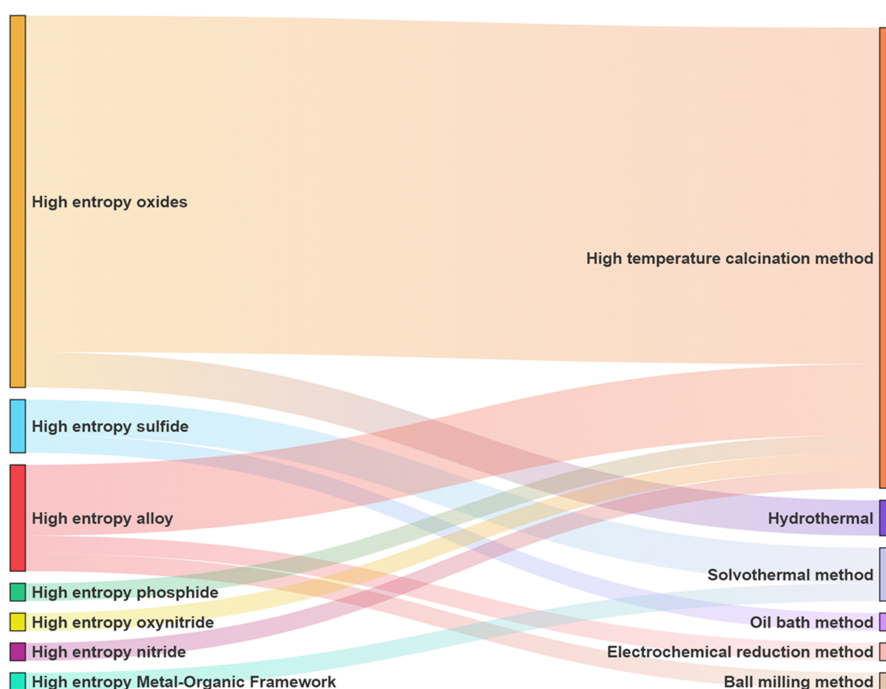


Figure 3. Distribution of types of HEPs and their synthesis strategies. HEPs: High entropy photocatalysts.

above, hydrothermal, solvothermal, oil bath, electrochemical reduction and ball milling methods are five other commonly used techniques for synthesizing HEPs, each with its own advantages and limitations. The hydrothermal method is carried out at low temperature and pressure, which is environmentally friendly and simple to operate, but the precise control of material composition is limited, and large-scale production may not be economical. The solvothermal method is performed at high temperatures and can precisely control the material composition and structure, but the use of organic solvents may bring environmental and safety issues and high costs. The oil bath method provides precise temperature control and is simple to operate, but it has high energy consumption and safety risks. The electrochemical reduction method can be conducted under mild conditions, saves energy, and is environmentally friendly, but it requires specific equipment and is complex to operate. The ball milling method uses mechanical force to mix element powders to improve the uniformity and stability of the catalyst. It is a dry powder operation and does not

require solvents, but it consumes a lot of energy and may contaminate the powder. When choosing a synthesis method, it is necessary to make a comprehensive consideration based on catalyst requirements, application scenarios, laboratory conditions and sustainability. Currently, among these five other synthesis strategies, hydrothermal/solvothermal methods are the two main synthesis strategies. Because they are very easy to achieve under laboratory conditions, they are favored by researchers, and are mainly used for the synthesis of high-entropy metal oxides and sulfides. Other multi-non-metal high-entropy materials and high-entropy alloys are unsuitable for these two methods.

ADVANTAGES OF HEPS IN THE FIELD OF PHOTOCATALYSIS

High-entropy materials offer several advantages in photocatalysis, making them promising candidates for various photocatalytic applications [Figure 4].

(1) Adjustability: the composition of high-entropy materials can be precisely tuned by adjusting the types and ratios of the constituent elements. This tunability allows researchers to tailor the energy band structure, electronic properties, and surface properties of high-entropy materials to optimize their photocatalytic performance for specific applications. In 2023, Wu *et al.* grew high-entropy metal tungstate (FeCoNiCuZn)WO₄ (named XWO₄) on polyacrylonitrile (PAN) nanofiber templates to construct composites for degradation of plastics^[37], and Figure 2A demonstrates that the energy band structure, the position of the center of the d-band, and the range of light absorption in PAN@XWO₄, as compared with PAN@ZnWO₄ and PAN@FeWO₄, acetic acid generation rate and selectivity were greatly enhanced, which reflects the tunability of HEPs.

(2) Broad spectrum absorption: High-entropy materials can be designed to exhibit broad-spectrum light absorption, covering wavelengths from ultraviolet (UV) to visible (Vis) and even near-infrared (NIR). This enables effective utilization of solar radiation for photocatalytic reactions, expanding the range of viable applications and improving energy efficiency. In 2024, Shi *et al.* synthesized the high-entropy metal sulfide (NiCdCuFeCo)S_x for the conversion of cellulose to generate carbon monoxide (CO) gas by solvothermal method^[38]. From Figure 4B, it can be clearly seen that the absorption of (NiCdCuFeCo)S_x samples from the UV region to the infrared light region was enhanced after the introduction of Ni, Cu, Fe, and Co elements, especially the enhancement of the absorption from the visible region to the infrared light region was more obvious. The above results indicate that the HEP can enhance the range and ability of light absorption of the material.

(3) Enhanced photocatalytic performance: High-entropy materials exhibit unique properties, including high compositional diversity and structural disorder, which can enhance photocatalytic activity compared to conventional materials. The presence of multiple elements in equimolar ratios creates a complex and dynamic environment for catalytic reactions, promoting synergistic effects and improving catalytic efficiency. The high degree of disorder and complexity of high-entropy materials promotes efficient charge separation and migration, which are key processes in photocatalysis. This facilitates the generation and transport of carriers (electrons and holes), reducing complex losses and improving overall photocatalytic efficiency. In 2021, Edalati *et al.* synthesized high-entropy metal oxide TiZrHfNbTaO₁₁ through high temperature calcination for water decomposition to produce H₂^[39]. It can be distinctly seen from Figure 4C that the H₂ production performance of the TiZrHfNbTaO₁₁ sample is significantly better than that of Ga₂ZnON₆. The above results show that HEPs can improve the photocatalytic ability of materials.

(4) Customizability: High-entropy materials are versatile in composition, structure, and morphology, allowing the design of photocatalysts according to specific catalytic requirements and environmental

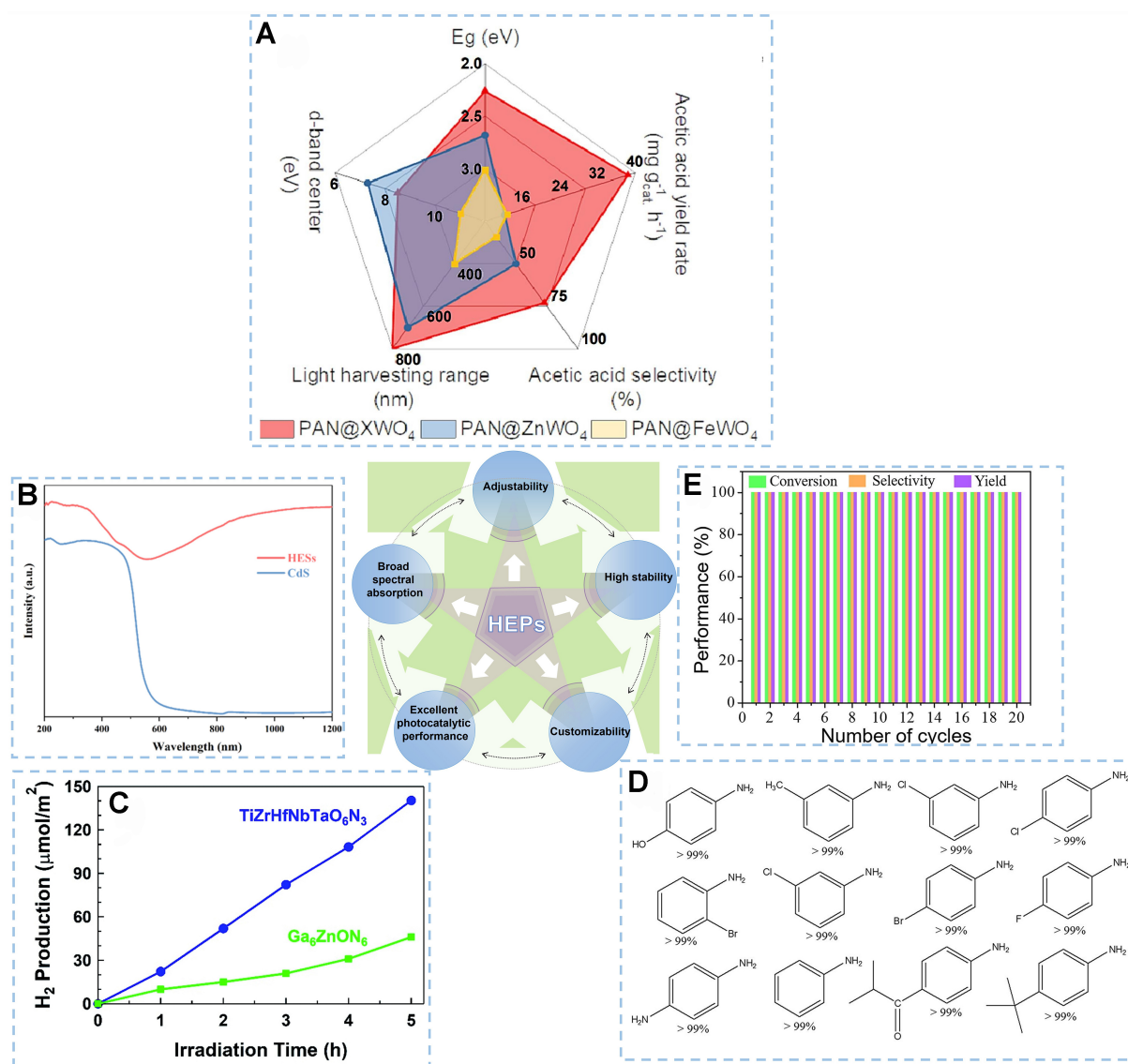


Figure 4. Some advantages of HEPs. (A) Adjustability^[37]; (B) Broad spectral absorption^[38]; (C) Excellent photocatalytic performance^[39]; (D) Customizability^[40]; and (E) High stability^[40]. HEPs: High entropy photocatalysts.

conditions. They can be synthesized using a variety of methods and tailored for different photocatalytic reactions, including pollutant degradation, water decomposition, carbon dioxide (CO₂) reduction, and organic synthesis. In 2021, Al Zoubi *et al.* constructed a high-entropy alloy CuAgNiFe for the conversion of nitrophenol compounds with some electron-withdrawing functional groups introduced on the phenol ring (e.g., -Cl, -I, and -CN), and high yields of aminophenol compounds (independent of the effects of different groups and positions) could be obtained on the CuAgFeNi catalysts^[40], and the above results indicate that HEPs can achieve the customization of the reaction for specific customizability of the reaction.

(5) High stability: High-entropy materials typically exhibit excellent thermal and chemical stability due to their high conformational entropy and structural robustness. This makes them resistant to degradation and performance deterioration under harsh reaction conditions, ensuring long-term stability and durability in photocatalytic applications. In 2021, Al Zoubi *et al.* constructed a high-entropy alloy CuAgNiFe that was

very stable in terms of conversion, selectivity, and yield for the reduction reaction of nitrophenol^[40], and the above results indicate that HEPs can be realized to construct catalysts with high stability and durability.

In addition, the unique properties of high-entropy materials provide opportunities to explore novel photocatalytic mechanisms and functions beyond conventional materials. This opens up possibilities for innovative applications and advances in areas such as energy conversion, environmental remediation, and chemical synthesis. Overall, high-entropy materials hold great promise for advancing photocatalysis by offering enhanced performance, tunable properties, and greater sustainability compared to conventional photocatalysts. Ongoing research efforts are focused on further understanding and optimizing the performance of high-entropy materials for a wide range of photocatalytic applications.

CHARACTERIZATION OF HEPS

Characterizing HEPs is essential to understanding their structure, composition, morphology, and photocatalytic properties [Figure 5]. Several characterization techniques are commonly employed to analyze high-entropy materials and assess their suitability for photocatalytic applications. Currently, X-ray diffraction (XRD) and high-resolution transmission electron microscopy (HRTEM) are mainly used to identify the crystalline phases present in HEPs and some other crystallographic parameters; characterizations such as scanning (SEM) and transmission electron microscopy (TEM) can observe the surface and internal structures of HEPs, including the nanoparticle morphology, particle size distribution, and agglomeration behaviors; and X-ray photoelectron spectroscopy (XPS) can identify the chemical compositions and oxidation states of the surface materials in HEPs, which can give insight into their surface reactivity and electronic structure; inductively coupled plasma (ICP) spectrometry, energy dispersive spectroscopy (EDS)/energy dispersive X-ray spectroscopy (EDX), *etc.* can determine the elemental composition of HEPs and provide quantitative information on the relative abundance of different elements. UV-Vis absorption spectroscopy and photoluminescence (PL) spectroscopy are essential characterization techniques for studying HEPs. UV-Vis absorption spectroscopy provides detailed information about the absorption peaks, which reflect the electronic structure and band gap of the material. This information is critical for evaluating the relationship between light absorption performance and photocatalytic activity. Metal-containing catalysts may exhibit surface plasmon resonance (SPR) effects, enhancing light absorption and catalytic activity. PL spectroscopy offers insights into the electronic excited states, analyzes the band structure, defect states, and evaluates photoelectric conversion and photocatalytic activity. Fluorescence lifetime analysis within PL spectroscopy aids in understanding the mechanisms of carrier transport and separation. Efficient PL signals are often associated with excellent photocatalytic performance. In summary, these characterization techniques play a crucial role in understanding the structure-performance relationship of HEPs and optimizing their performance for various photocatalytic applications. By combining multiple characterization methods, researchers can gain a comprehensive understanding of the composition, structure, morphology, optical properties, and catalytic behaviors of HEPs; however, more detailed structural characterization of HEPs still needs to be explored further. Furthermore, density-functional theory (DFT) has been widely applied in the field of HEPs, which is mainly used for: calculating the predicted electronic structure and energy band structure to analyze the photoelectron conversion mechanism; predicting the light absorption performance and optimizing the absorption characteristics; investigating the active site and surface reaction mechanism to understand the active center of the catalysts; analyzing the effect of defect structure on electron transport and carrier separation; evaluating the stability and predicting the photocatalytic performance and screening of effective catalysts. As a theoretical computational tool, DFT is of great significance for the design, optimization and application of HEPs, and its role will become more significant with the improvement of computational capability and model development to promote the development of high-efficiency catalysts.

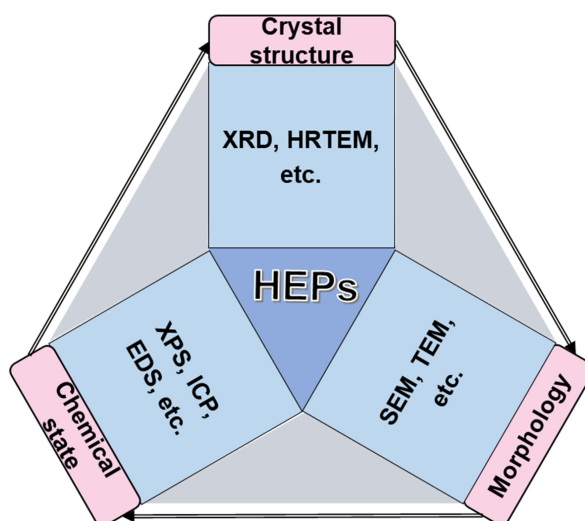


Figure 5. Some characterization methods for HEPs. HEPs: High entropy photocatalysts.

DESIGN OF HEPs

In order to construct HEPs with efficient photocatalytic performance, it is a very arduous task to screen them only by traditional experiments, and a series of detailed and regular data cannot be obtained. Therefore, a comprehensive database of HEPs is needed to link the composition, structure, reaction process and activity to screen and prepare the optimal HEPs [Figure 6]. By combining high-throughput screening and ML, we can design highly active HEP materials with appropriate adsorption energies faster. Considering the coordination effect (different crystalline surfaces and defects exposure) and ligand effect (spatial arrangement of different elements), many teams have built various models [e.g., ML model, artificial neural network (ANN), support vector machine (SVM), *etc.*] to predict the HEP materials, which will also involve molecular dynamics (MD) and DFT, and finally, we can get satisfactory HEP materials. It is only in the end that a satisfactory combination of elements may be obtained^[41–46]. Further, the above ML models are not chosen arbitrarily, which is related to the actual experimental data, and the experimental information will support the creation of more appropriate models. In particular, the adsorption sites of HEPs are quite complex, which requires scholars to consider all atomic coordination environments on the surface of HEP materials as carefully as possible^[28,47,48]. Therefore, there is a long way to go to predict and develop HEPs through theoretical calculations combined with ML.

APPLICATIONS OF HEPs IN THE FIELD OF ENERGY AND ENVIRONMENT

HEPs have begun to receive widespread attention as emerging materials in the field of photocatalysis. The catalytic principle of HEPs is grounded in their unique characteristics, including the uniform distribution of multiple elements, numerous surface active sites, excellent light absorption, and superior electron transport properties. These catalysts are composed of at least five elements mixed in nearly equimolar ratios to form a solid solution. This configuration enhances stability and activity while increasing the number of surface active sites. HEPs exhibit strong light absorption capabilities in both the Vis and UV regions, which promotes the generation of excited state electrons. Their complex electronic and lattice structures facilitate accelerated electron transport and effective separation of photogenerated electron-hole pairs, thereby improving reaction efficiency. The high-entropy design also reduces the reaction activation energy, increasing the reaction rate and selectivity. Together, these attributes provide HEPs with exceptional performance in photocatalysis, advancing technological development and practical applications. As shown in Figure 7, at present, HEPs are still mainly concentrated in the fields of degradation (41.7%) and H_2/O_2

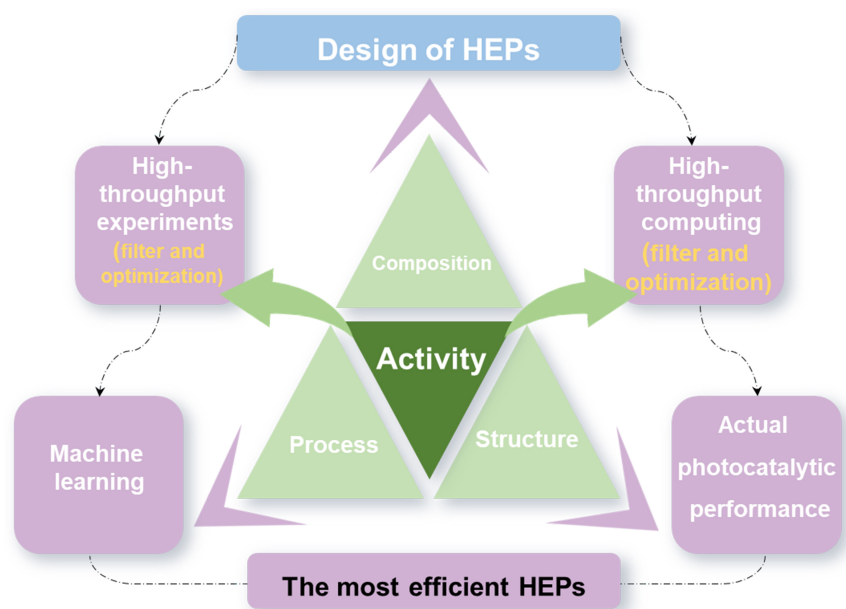


Figure 6. High-throughput screening and ML for predicting HEPs. ML: Machine learning; HEPs: high entropy photocatalysts.

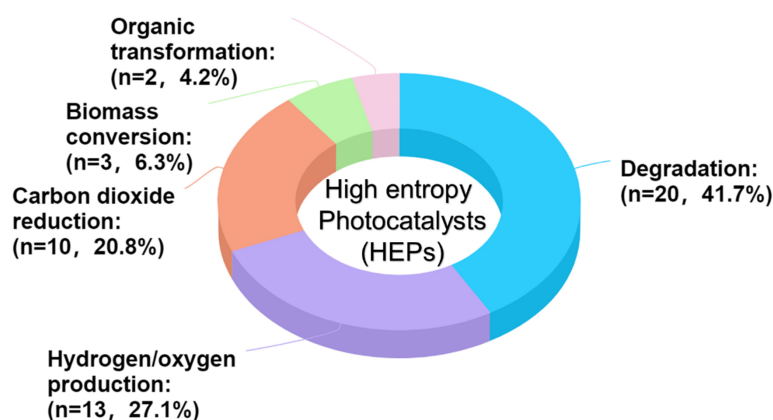


Figure 7. Application of HEPs in various photocatalytic fields. HEPs: High entropy photocatalysts.

production (27.1%), which may be attributed to the relatively early development of these two fields, while for other reaction systems with selectivity requirements (CO_2 reduction, biomass conversion, and organic synthesis) have already demonstrated their strong advantages, which have been greatly improved by designing HEPs with high yields of target products. Further, we believe that HEPs will also show impressive results in other photoreaction systems, such as methane (CH_4) oxidation and N_2 fixation.

Degradation

HEPs offer several advantages in the field of pollutant degradation for the removal of harmful pollutants from water and soil environments. They can be customized for a wide range of contaminants, including organic (e.g., difficult-to-degrade organic compounds, pesticides, dyes) and emerging contaminants (e.g., personal care products, pharmaceuticals). This versatility allows for the effective removal of a wide range of contaminants from a variety of environmental matrices^[49–57]. HEPs can exhibit selective catalytic activity for specific pollutant degradation reactions, contributing to targeted removal of priority pollutants while

minimizing degradation of non-target compounds. They promote the complete mineralization of contaminants into harmless by-products such as water, CO₂ and inorganic salts. This minimizes the formation of undesirable intermediates and by-products, reducing the potential for secondary contamination and environmental impact. Overall, HEPs hold great promise for advancing pollutant degradation technologies by providing efficient, selective, and sustainable solutions for environmental remediation. Fu *et al.* constructed (Bi_{0.2}Na_{0.2}Ba_{0.2}K_{0.2}La_{0.2})TiO₃ (BNBKL) for the degradation of organic pollutants [rhodamine B (RhB)] by the ball milling method combined with calcination^[58], and the EDS-mapping results in Figure 8A indicate that seven elements (Bi, K, Ba, Ti, Na, La, and O) are uniformly distributed in the sample, and the introduction of these A-site metal ions will lead to lattice distortion and a certain entropy value. The introduction of these A-site metal ions will lead to the lattice distortion of the octahedron with a certain entropy value. The degradation rates of RhB by BNBKL were 7.65×10^{-3} and $6.85 \times 10^{-3} \text{ min}^{-1}$ under Vis and UV conditions, respectively. Further, the degradation rates of BNBKL under piezoelectric-photocatalytic conditions were 19.05×10^{-3} and $24.26 \times 10^{-3} \text{ min}^{-1}$ under Vis and UV conditions, respectively. Degradation rates under piezoelectric-photocatalytic conditions were 19.05×10^{-3} and $24.26 \times 10^{-3} \text{ min}^{-1}$ for Vis and UV light conditions, respectively, indicating that the degradation rate under piezoelectric-photocatalytic conditions was greater than the sum of piezoelectric- or photocatalytic-degradation rates alone, or photocatalytic degradation rate alone, showing a synergistic effect. The BNBKL [Figure 8B] achieved 98% RhB degradation in 120 min. In addition, the degradation efficiencies of BNBKL for cationic dyes [methyl orange (MO)] and anionic dyes [methylene blue (MB) and amido black 10B (AB10B)] were 98%, 73%, and 46%, respectively, showing its degradation ability for different types of dyes. These data collectively reflect the performance of BNBKL in photocatalytic and piezoelectric-photocatalytic degradation of organic pollutants, which is mainly due to the introduction of various metal ions in the structure of BNBKL leading to a richer number of active sites, and at the same time, these ions also cause a certain degree of lattice distortion and energy band reduction (light absorption enhancement), which, in turn, exhibits a significant enhancement of piezoelectric photo-degradation. Jia *et al.* showed a significant enhancement of piezoelectric photo-degradation of RhB through a sol-gel method combined with calcination. (La_{0.2}Ce_{0.2}Gd_{0.2}Zr_{0.2}Fe_x)O₂ was prepared through sol-gel method combined with calcination^[59], and the results of EDS-mapping [Figure 8C] showed a uniform distribution of six elements (La, Ce, Gd, Zr, Fe, and O), indicating the formation of entropically stabilized structures. Comparative results of the degradation of tetracycline hydrochloride (TCH) by introducing samples with different contents of Fe elements show that the introduction of suitable concentration of Fe elements can greatly enhance its degradation efficiency, in which the degradation rate of H-1 was increased from 50.9% (H-0) to 95.4% at 3 h [Figure 8D]. In particular, the degradation efficiency of H-1 reached 96.3% at pH 7.00. The light absorption performance of H-1, H-2 and H-3 samples in the visible range was better than that of H-0 samples, which was attributed to the high entropy effect and changes in the energy band structure. Finally, a photocatalytic mechanism diagram was proposed [Figure 8E], in which $\cdot\text{O}_2^-$ and $\cdot\text{OH}$ generated by the HEP (La_{0.2}Ce_{0.2}Gd_{0.2}Zr_{0.2}Fe_x)O₂ under light illumination could mineralize TCH into H₂O and CO₂. Das *et al.* synthesized FeCoNiCuZn high-entropy alloy through the calcination method and used it to degrade antibiotics, and achieved very good results^[60]. The degradation efficiencies of FeCoNiCuZn high-entropy alloys for four different pharmaceutically active compounds (PhACs) under visible light irradiation were 86% for tetracycline (TC), 94% for sulfamethoxazole (SMX), 80% for ibuprofen (IBP), and 99% for diclofenac (DCF). This is mainly because the high concentration of $\cdot\text{O}_2^-$ and $\cdot\text{OH}$ generated by FeCoNiCuZn alloy under light conditions can effectively mineralize these antibiotics [Figure 8F]. Das *et al.* also synthesized MnFeCoNiCu high-entropy alloy nanoparticles for photodegradation of various antibiotics by ball milling plus calcination^[61], in which the removal effects of ciprofloxacin (CFX, 89%), ofloxacin (OFX, 94%) and SMX (95%) were very significant. Further, the total organic carbon (TOC) removal of OFX, CFX and SMX by MnFeCoNiCu high-entropy alloy nanoparticles was 74%, 71% and 66%, respectively. This was mainly due to the fact that the MnFeCoNiCu alloy was generated by light to generate high concentrations of

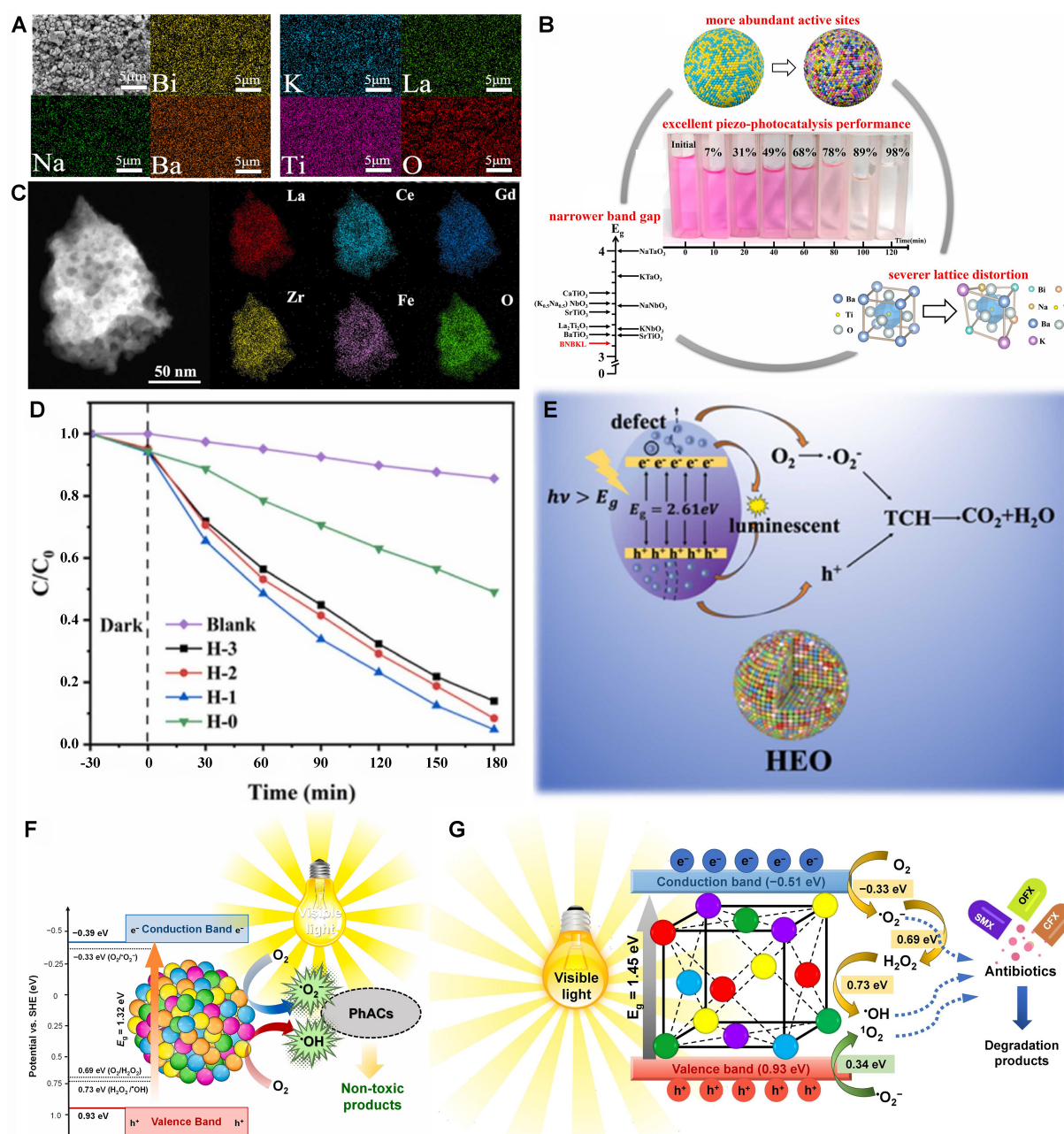


Figure 8. (A) EDS mapping of BNBKL; (B) Schematic diagram of the photocatalytic performance of BNBKL HEPO powder and the advantages of HEPO (more active sites, severe Lattice distortion, narrower band gap). Reproduced with approval^[58]. Copyright 2024, Elsevier; (C) EDS mapping of $(\text{La}_{0.2}\text{Ce}_{0.2}\text{Gd}_{0.2}\text{Zr}_{0.2}\text{Fe}_{0.05})\text{O}_2$; (D) Different $(\text{La}_{0.2}\text{Ce}_{0.2}\text{Gd}_{0.2}\text{Zr}_{0.2}\text{Fe}_{0.05})\text{O}_2$ samples for removal of TCH; (E) Photodegradation mechanism diagram of $(\text{La}_{0.2}\text{Ce}_{0.2}\text{Gd}_{0.2}\text{Zr}_{0.2}\text{Fe}_{0.05})\text{O}_2$. Reproduced with approval^[59]. Copyright 2024, Elsevier; (F) Mechanism diagram of the photodegradation of various antibiotics by FeCoNiCuZn alloy. Reproduced with approval^[60]. Copyright 2023, Elsevier; (G) Mechanism diagram of the photodegradation of various antibiotics by MnFeCoNiCu alloy. Reproduced with permission^[61]. Copyright 2023, Elsevier. EDS: Energy dispersive spectroscopy; BNBKL: $(\text{Bi}_{0.2}\text{Na}_{0.2}\text{Ba}_{0.2}\text{K}_{0.2}\text{La}_{0.2})\text{TiO}_3$; HEPO: high-entropy perovskite oxides; TCH: tetracycline hydrochloride.

$\text{O}_2^{\cdot-}$, OH^{\cdot} and $\text{O}_2^{\cdot-}$ to go back to attack these antibiotics to achieve the degradation effect [Figure 8G]. The above results further indicate that various types of HEPs will show attractive results in the field of photocatalytic degradation. As can be seen from Table 1, the current application of HEPs in the field of pollutant degradation is mainly some colored pollutants and antibiotics. The application of degradation of

Table 1. Different HEPs for degradation of organic pollutants

HEPs	Application	Condition	Performance	Ref.
CuCoMnO _x /ZnO	Degradation of MB	A LED flashlight with a power density of 50 mW·cm ⁻²	53.84% degradation of MB in 120 min	[49]
(Co, Mg, Ni, Cu, Zn) _{1-x} Ca _x O (x = 0.05, 0.1)	Degradation of MB	A 100 mW·cm ⁻² solar simulator	97% decomposition of MB in 80 min	[50]
(Fe _{0.5} Co _{0.5}) ₇₀ B ₂₁ Ta ₄ Ti ₅	Degradation of EY	300 W high-voltage mercury lamp with UV-light	100% decomposition of EY in 120 min	[51]
Pb _x Cd _{1-x} BiO ₂ Br	Degradation of RhB, CIP, TC	250 W xenon lamp	-	[53]
(La _{0.2} Nd _{0.2} Sm _{0.2} Gd _{0.2} Y _{0.2}) ₂ Zr ₂ O ₇	Degradation of RhB	A long arc mercury lamp (CELLAM500)	90.8% decomposition of RhB in 120 min	[55]
(La _{0.2} Nd _{0.2} Sm _{0.2} Gd _{0.2} Y _{0.2}) ₂ Zr ₂ O ₇	Degradation of RhB	UV lamp	70% decomposition of RhB in 120 min	[56]
(Ni ₄₀ Fe ₃₀ Co ₂₀ Al ₁₀) ₉₀ Ti ₁₀	Degradation of MB	300 W Xe lamp	100% decomposition of MB in 180 min	[57]
(Bi _{0.2} Na _{0.2} Ba _{0.2} K _{0.2} La _{0.2})TiO ₃	Degradation of RhB, MB, MO, AB10B	Ultrasound stimuli (150 W, 40 kHz), light irradiation (Xe lamp, 300 W)	100% degradation of RhB in 120 min, 73% decomposition of MB in 120 min, 46% decomposition of MO in 120 min, 98% degradation of AB10B in 120 min	[58]
(La _{0.2} Ce _{0.2} Gd _{0.2} Zr _{0.2} Fe _x)O ₂	Degradation of TC	300 W xenon lamp, with a cut-off filter at 420 nm	95.4% degradation of TC in 180 min	[59]
FeCoNiCuZn HEA	Degradation of TC, SMX, IBP, and DCF	450 W high-pressure mercury vapor lamp	86% degradation of TC in 120 min, 94% decomposition of SMX in 120 min, 80% decomposition of IBP in 120 min, 99% degradation of DCF in 120 min	[60]
MnFeCoNiCu-based high entropy alloy	Degradation of SMX, OFX and CFX	450 W high-pressure mercury vapor lamp, equipped with UV cutoff filter	95% degradation of SMX in 120 min, 94% decomposition of OFX in 120 min, 89% decomposition of CFX in 120 min	[61]
(Mn _{0.2} Fe _{0.2} Co _{0.2} Ni _{0.2} Cu _{0.2}) ₃ O ₄	Degradation of TCH	300 W xenon lamp with the 420 nm UV cut-off filter	92.9% decomposition of TCH in 60 min	[62]
(CaxZrYCeCr)O ₂ (x = 0.09-0.5)	Degradation of MB	150-W Xe lamp, ultrasonic vibration (at 40 kHz and 250 W)	100% degradation of MB in 60 min	[63]
NiAl ₂ O ₄ /FeCoNiCrTi	Degradation of TC	300 W Xe lamp	84.6% degradation of TC in 120 min	[64]
NbTaZrMoW high-entropy alloys	Degradation of MB	300 W Ultra-Vitalux lamp	58.77% decomposition of MB in 180 min	[65]
(FeCoNiCuZn) _a O _b	Degradation of SMX, OFX	250 W high-pressure mercury vapor lamp (with UV cutoff)	97% degradation of SMX in 90 min, 95% degradation of OFX in 90 min	[66]
BiO[ClBrI(CO ₃) _{0.5}]	Degradation of MO	300 W xenon lamp (λ > 400 nm)	100% degradation of MO in 20 min	[67]
(Na _{0.5} K _{0.5})(Sr _{0.4} Ba _{0.3} Ca _{0.3}) ₂ Nb ₅ O ₁₅	Degradation of MB	400-watt xenon lamp was combined with a full-wavelength reactor and filter (AM 1.5) to simulate sunlight (300-1,100 nm)	-	[68]
(Co _{0.2} Mn _{0.2} Fe _{0.2} Cr _{0.2} Cu _{0.2}) ₃ O ₄	Degradation of MB	Xe lamp	-	[69]
Ce _{0.2} Zr _{0.2} La _{0.2} Pr _{0.2} Y _{0.2} O ₂	Degradation of MB, MO, RhB, MR	300 W ozone free xenon lamp equipped with an AM 1.5 filter (Newport 66902)	98.9% degradation of MB in 20 min, 100% decomposition of MO in 20 min, 100% decomposition of RhB in 20 min, 100% degradation of MR in 20 min	[70]

HEPs: High entropy photocatalysts; MB: methylene blue; LED: light-emitting diode; EY: Eosin Y; UV: ultraviolet; RhB: rhodamine B; CIP: ciprofloxacin; TC: tetracycline; MO: methyl orange; AB10B: amido black 10B; TC: tetracycline; SMX: sulfamethoxazole; IBP: ibuprofen; DCF: diclofenac; OFX: ofloxacin; CFX: ciprofloxacin; TCH: tetracycline hydrochloride; MR: methyl red.

other organic pollutants has not yet been fully launched and still requires more exploration.

H₂/O₂ production

HEPs offer several advantages in the field of water decomposition, which involves the conversion of water into H₂ and O₂ using solar energy. The effective absorption of sunlight by HEPs promotes the activation of water molecules and facilitates energy-efficient conversion processes. HEPs can exhibit selective catalytic activity for specific water splitting reactions (mainly H₂ and, to a lesser extent, O₂)^[63,71-75]. The composition

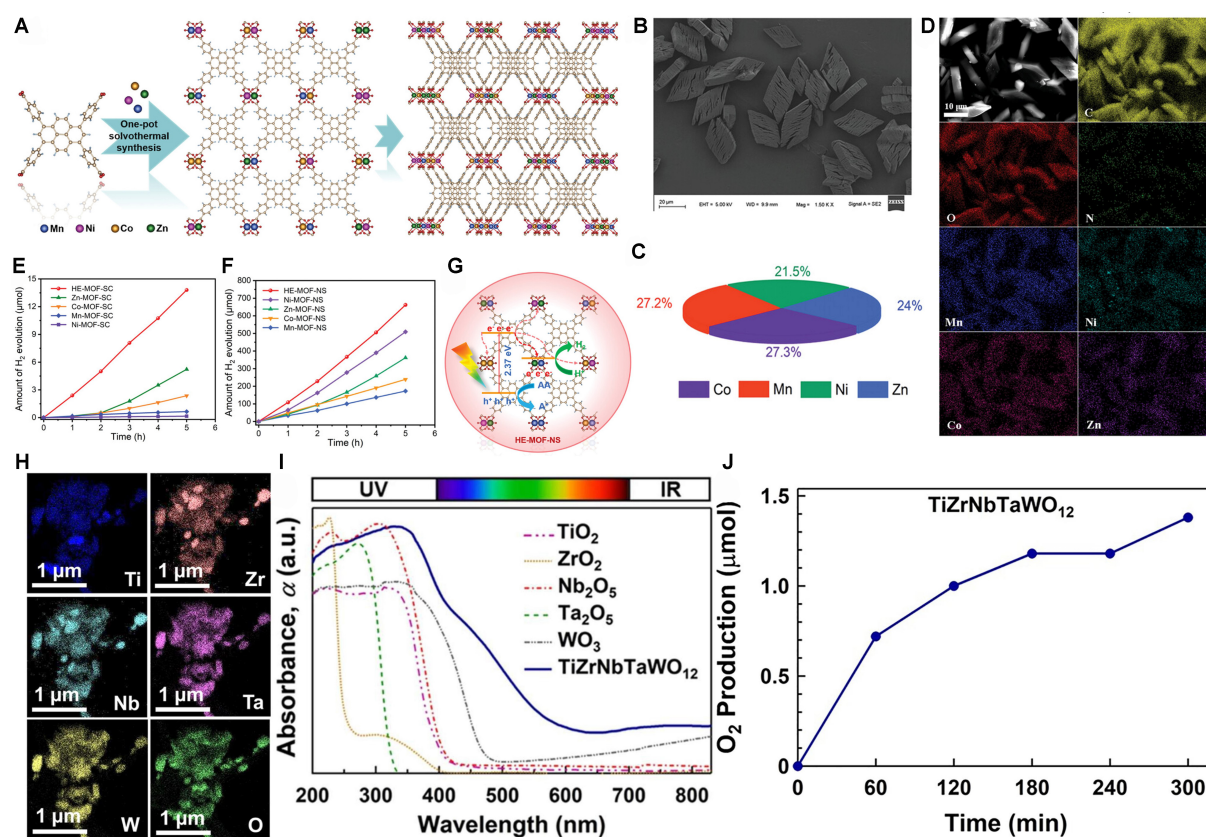


Figure 9. (A) Schematic of the synthesis process and structure of HE-MOF-SC; (B) SEM image of HE-MOF-SC; (C) Metal compositions (molar ratios) of HE-MOF-SC were calculated from ICP-AES results; (D) SEM-EDX elemental distribution of C, O, N, Ni, Co, Mn and Zn for HE-MOF-SC; (E) Time course of photocatalytic H_2 precipitation over Ni (or Mn or Co or Zn)-MOF-SC and HE-MOF-SC photocatalysts; (F) Time course of photocatalytic H_2 precipitation over Ni (or Mn or Co or Zn)-MOF-NS, and HE-MOF-NS photocatalysts; (G) Schematic representation of the relative energy levels of ligands and nodes, electron transfer pathways, and photocatalytic H_2 production mechanism. Reproduced with approval^[76]. Copyright 2023, Wiley; (H) EDS-mapping diagram of TiZrNbTaWO_{12} ; (I) compared with related binary oxides, the range of light absorption capacity of TiZrNbTaWO_{12} ; (J) photocatalytic O_2 production performance of TiZrNbTaWO_{12} . Reproduced with permission^[77]. Copyright 2022, Elsevier. HE-MOF-SC: High-entropy metal-organic framework single crystal; SEM: scanning electron microscopy; ICP-AES: inductively coupled plasma-atomic emission spectrometry; EDX: energy dispersive X-ray spectroscopy; HE-MOF-NS: high-entropy metal-organic framework nanosheets; EDS: energy dispersive spectroscopy.

and structure of HEPs can be precisely adjusted to optimize their water splitting performance. By adjusting the types and ratios of the constituent elements, researchers can tailor the energy band structure, electronic properties, and surface features of HEPs to enhance their activity, selectivity, and stability in hydrolysis reactions. Overall, HEPs hold great promise for advancing water splitting technology by providing an efficient, selective, and sustainable pathway for H_2 production from solar energy. Qi *et al.* synthesized the high-entropy MOF single crystal (HE-MOF-SC) material by one-pot solvent heating, and then exfoliated it to form the 2D high-entropy MOF nanosheets (HE-MOF-NS) material by solvent intercalation [Figure 9A]^[76]. The results of the SEM image [Figure 9B] showed that the HE-MOF-SC exhibits a rhombic structure, and the results of the ICP-atomic emission spectrometry (AES) indicated that the ratio of metal atoms is not much different from the theoretical value, suggesting that these different metal ions have been stabilized in the MOF structure [Figure 9C]. Further, the results of EDX-mapping of HE-MOF-SC [Figure 9D] indicate that its meso-elements (Co, Zn, Mn, Ni, O, C, N) are uniformly distributed in the sample. Under visible light irradiation, the photocatalytic H_2 release rate of HE-MOF-SC is $2.76 \mu\text{mol}\cdot\text{h}^{-1}$, while the rate for HE-MOF-NS is $132.4 \mu\text{mol}\cdot\text{h}^{-1}$, which is 48 times higher than that of HE-MOF-SC. In comparison,

the rates for Ni-MOF-SC, Mn-MOF-SC, Co-MOF-SC, and Zn-MOF-SC are 0.03, 0.13, 0.47, and 1.04 $\mu\text{mol}\cdot\text{h}^{-1}$, respectively. The activities for Ni-MOF-NS, Mn-MOF-NS, Co-MOF-NS, and Zn-MOF-NS are 101.8, 34.5, 47.8, and 72.4 $\mu\text{mol}\cdot\text{h}^{-1}$, respectively, all of which are lower than that of HE-MOF-NS. HE-MOF-NS can achieve efficient photocatalytic H_2 evolution reaction (HER) in aqueous solution without the need for a co-catalyst, demonstrating an activity that surpasses most water-stable MOF catalysts [Figure 9E and F]. A mechanism diagram as in Figure 9G is proposed, where more photogenerated electrons are formed from the ligand structure by photoexcitation and migrate to multiple metal ions to form a high-entropy structure through the ligand-to-metal charge transfer process, which, as the main active site for photocatalytic H_2 precipitation, substantially enhances the photocatalytic H_2 production performance. Edalati *et al.* synthesized TiZrNbTaWO_{12} high-entropy material by high temperature calcination method, and the results of EDS-mapping [Figure 9H] showed that the six elements in the sample were uniformly distributed and the light absorption range of the sample was significantly enhanced [Figure 9I]. Compared to binary oxides such as TiO_2 , ZrO_2 , Nb_2O_5 , Ta_2O_5 , and WO_3 , the TiZrNbTaWO_{12} high-entropy material exhibits a higher photocatalytic activity (without the need for co-catalyst additions), with an O_2 production of 12.1 $\mu\text{mol}\cdot\text{h}^{-1}\cdot\text{g}^{-1}$ [Figure 9J]. This performance is attributed to the high visible light absorption, low band gap, proper energy band structure, presence of multiple heterojunctions and the resulting easy separation and slow complexation of electron-holes^[77]. As can be seen from Table 2, the H_2 production of HEPs as the main catalysts is not high, and only some samples reach the mmol level of the H_2 production rate, but many of them realize the effect of H_2 and O_2 production without co-catalysts. Based on the overall low performance, more exploration is still needed to improve the overall H_2 and O_2 production efficiency.

CO₂ reduction

HEPs offer several advantages in the field of CO_2 reduction, including the use of solar energy to convert CO_2 into value-added products such as fuels, chemicals, and feedstocks. The effective absorption of sunlight by HEPs promotes the activation of CO_2 molecules and facilitates energy-efficient conversion processes. The tunability of HEPs can be tailored to exhibit selective catalytic activity for specific CO_2 reduction reactions, such as the production of CO, CH_4 , methanol (CH_3OH) or other hydrocarbons and oxygenates^[78,82,83]. Overall, HEPs hold great promise for advancing CO_2 abatement technologies by providing an efficient, selective, and sustainable pathway to utilize solar energy to convert CO_2 into valuable products. Continued research and development efforts in this area are expected to lead to the commercialization of HEPs for CO_2 abatement applications and the transition to a carbon-neutral economy. Zhang *et al.* prepared $(\text{NiCuMnCoZnFe})_3\text{O}_4$ high-entropy hollow porous nanotubes (HESO NFs) by electrostatic spinning coupled with calcination, with a diameter of about 290 nm [Figure 10A]^[84]. The results of HRTEM [Figure 10B] and selected-area electron diffraction [Figure 10C] indicate the presence of a variety of randomly oriented nanocrystalline structures in the material, and the EDS-mapping results [Figure 10D] show that each metal element is uniformly distributed and in close proximity to each other. HESO NFs have a certain ability to reduce CO_2 to produce CO (42.8 $\mu\text{mol}\cdot\text{g}^{-1}\cdot\text{h}^{-1}$) and CH_4 (8.7 $\mu\text{mol}\cdot\text{g}^{-1}\cdot\text{h}^{-1}$) [Figure 10E]. A mechanism diagram was proposed as in Figure 10F, where the high entropy effect of $(\text{NiCuMnCoZnFe})_3\text{O}_4$ promotes efficient carrier migration and thus enhances the photocatalytic activity. Akrami *et al.* synthesized $\text{TiZrNbHfTaO}_6\text{N}_3$ high-entropy material with polycrystalline structure and a very homogeneous distribution of the elements by calcination [Figure 10G]^[85]. $\text{TiZrNbHfTaO}_6\text{N}_3$ has the highest photocatalytic reduction of CO_2 to produce CO (average value of CO after 5 h at $1.6 \pm 1.5 \mu\text{mol}\cdot\text{g}^{-1}\cdot\text{h}^{-1}$) [Figure 10H]. Jiang *et al.* synthesized $(\text{Ga}_{0.2}\text{Cr}_{0.2}\text{Mn}_{0.2}\text{Ni}_{0.2}\text{Zn}_{0.2})_3\text{O}_4$ high-entropy material by a combination of a water bath and calcination method^[86]. The products of CO_2 reduction in aqueous solution were dominated by H_2 , CO and CH_4 , among which the $(\text{Ga}_{0.2}\text{Cr}_{0.2}\text{Mn}_{0.2}\text{Ni}_{0.2}\text{Zn}_{0.2})_3\text{O}_4$ material (GSHEO-800) generated by calcination at 800 °C showed the best performance (H_2 , 47.36 $\mu\text{mol}\cdot\text{g}_{\text{cat}}^{-1}\cdot\text{h}^{-1}$; CO, 23.01 $\mu\text{mol}\cdot\text{g}_{\text{cat}}^{-1}\cdot\text{h}^{-1}$; CH_4 , 2.89 $\mu\text{mol}\cdot\text{g}_{\text{cat}}^{-1}\cdot\text{h}^{-1}$) [Figure 10I]. As can be seen on the mechanistic diagram in Figure 10J, the energy band

Table 2. Different HEPs for H₂/O₂ production

HEPs	Application	Condition	Performance	Ref.
Pt ₁₈ Ni ₂₆ Fe ₁₅ Co ₁₄ Cu ₂₇ nano-high-entropy alloy	H ₂ generation	LED light source (λ = 420 nm, 67.7 mW·cm ⁻²)	H ₂ production (2.4 mmol·g ⁻¹ ·h ⁻¹)	[29]
TiZrHfNbTaO ₆ N ₃	H ₂ generation	300 W Xe lamp	-	[39]
(Ca _x Zr _{1-x} YCeCr)O ₂ (x = 0.09-0.5)	H ₂ generation	150-W Xe lamp, ultrasonic vibration (at 40 kHz and 250 W)	H ₂ production (677 μmol·g ⁻¹ ·h ⁻¹)	[63]
Ce _{0.2} Zr _{0.2} La _{0.2} Pr _{0.2} Y _{0.2} O ₂	H ₂ generation	300 W ozone free xenon lamp equipped with an AM 1.5 filter (Newport 66902)	H ₂ production (9.2 μmol·mg ⁻¹ ·h ⁻¹)	[70]
Ag(CuZn)(AlCr) ₂ O ₄ /CuO	H ₂ generation	300 W 40 kHz Ultrasonic + 300 W Xe lamp	H ₂ production (1,716 μmol·g ⁻¹ ·h ⁻¹)	[71]
High-entropy metal phosphides/ZnIn ₂ S ₄	H ₂ generation	300 W xenon lamp (CEL-HXF300)	H ₂ production (4,630.21 μmol·g ⁻¹ ·h ⁻¹)	[73]
TiHfZrNbTaO ₁₁	H ₂ generation	300 W Xe lamp	-	[75]
HE-MOF-NS	H ₂ generation	300W Xe-lamp (Perfect Light, PLS-SXE 300) with a 420 nm cutoff filter	H ₂ production (132.4 μmol·h ⁻¹)	[76]
TiZrNbTaWO ₁₂	O ₂ generation	300 W Xe lamp (PE300BUV, Perkin Elmer) equipped with a 420 nm cut-off filter	O ₂ production (12.1 μmol·g ⁻¹ ·h ⁻¹)	[77]
TiZrNbHfTaO ₁₁	H ₂ generation	High-pressure Hg light source (Sen Lights Corporation, HL400BH-8, 400 W)	-	[78]
Li(HE)O ₃ (HE, Nb:V:Ta:Cr:Mo:W:Co = 0.5:0.083:0.083:0.083:0.083:0.083:0.083)	H ₂ generation	AM 1.5G	H ₂ production (6.61 mmol·g ⁻¹ ·h ⁻¹)	[79]
TiZrNbHfTaO _x	H ₂ generation	300 W Xe lamp	H ₂ production (134.76 μmol·m ⁻² ·h ⁻¹)	[80]
TiZrNbHfTaO ₁₁	H ₂ generation	High-pressure mercury light source (500 mW·cm ⁻²)	H ₂ production (990 μmol·g ⁻¹ ·h ⁻¹)	[81]

HEPs: High entropy photocatalysts; LED: light-emitting diode; HE-MOF-NS: high-entropy metal-organic framework nanosheets.

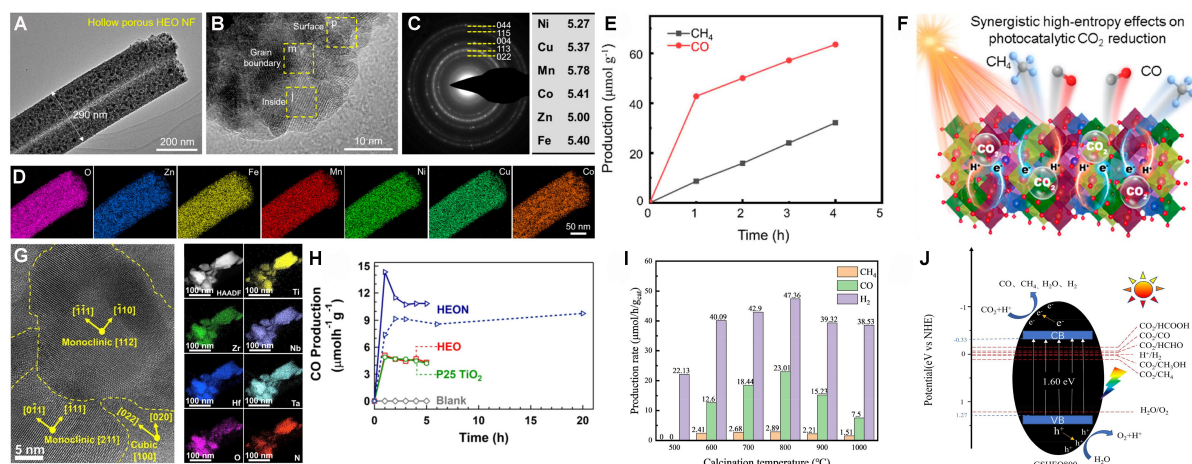


Figure 10. (A and B) TEM, (C) SEAD, (D) EDS-mapping of hollow porous spinel (NiCuMnCoZnFe)₃O₄ NF (400 °C); (E) Photocatalysis product of (NiCuMnCoZnFe)₃O₄ NF (400 °C) catalyst; (F) Mechanism diagram of synergistic (NiCuMnCoZnFe)₃O₄ NF (400 °C) photoreduction of CO₂ to generate CH₄ and CO. Reproduced with approval [84]. Copyright 2024, American Chemistry Society; (G) HRTEM image and EDS-mapping image of TiZrNbHfTaO₆N₃; (H) Effect image of TiZrNbHfTaO₆N₃ and some other comparative samples photoreducing CO₂ to generate CO. Reproduced with permission [85]. Copyright 2022, Elsevier; (I) Product formation rate diagram of photoreduction of CO₂ by (Ga_{0.2}Cr_{0.2}Mn_{0.2}Ni_{0.2}Zn_{0.2})₃O₄ synthesized under different temperature conditions; (J) Energy band structure of GSHEO800 and mechanism diagram of photoreduction of CO₂. Reproduced with permission [86]. Copyright 2023, Elsevier. TEM: Transmission electron microscopy; SEAD: selected area diffraction; EDS: energy dispersive spectroscopy; NF: nanofiber; HRTEM: high-resolution transmission electron microscopy.

position of GSHEO-800 meets all the conditions for CO₂ reduction, and the generation of H₂ in the reaction system hinders the reduction of CO₂, which stays at the stage of the main product of CO, while the kinetic conditions for the generation of CH₄ are much more difficult leading to the generation of a small amount of CH₄. From Table 3, it can be seen that the main products of photoreduction of CO₂ by HEPs are still CO and CH₄, and the generation efficiency of these two products is not high at present, and there is still a need to take advantage of the characteristics of HEPs with multiple active sites to enhance their efficiency in generating specific products.

Biomass conversion

HEPs offer several advantages in biomass conversion processes, which involve the conversion of biomass-derived feedstocks into value-added products such as biofuels, chemicals, and materials. They can be adapted to a wide range of biomass feedstocks, including lignocellulosic biomass, agricultural residues, wastes, and biomass-derived intermediates (the main ones that have been investigated so far are sugars and cellulose)^[38,87,90]. This versatility enables the utilization of a wide range of biomass resources for sustainable and renewable production processes. HEPs can exhibit selective catalytic activity for specific biomass conversion reactions such as biomass depolymerization, dehydration, hydrogenation and upgrading. Their composition, structure, and surface properties can be optimized to facilitate desired reaction pathways and minimize unwanted side reactions. Overall, HEPs hold great promise for advancing biomass conversion technologies by providing efficient, selective, and sustainable pathways to convert biomass feedstocks into valuable products. Continued research and development efforts in this area are expected to lead to the commercialization of HEPs for biomass conversion applications and a more sustainable and circular bioeconomy. In 2024, Shi *et al.* constructed (NiCdCuFeCo)_x HEPs by solvothermal method, and the diffraction peaks of the XRD were consistent with the results of the simulated data [Figure 11A], and the results of the EDX-mapping [Figure 11B] showed that the six elements (Ni, Cd, Cu, Fe, Co, and S) were uniformly distributed in the sample^[38]. Further, the results of ICP [Figure 11C] showed that the content of five metal elements (Cd, Cu, Fe, Ni, Co) decreased in order. The (NiCdCuFeCo)_x constructed by the above results is a high-entropy material. Based on gas chromatography (GC) analysis, CO was found to be the major product of cellulose conversion [Figure 11D]. Notably, compared to other metal sulfides with relatively simple compositions (i.e., composed of one to four elements), (NiCdCuFeCo)_x exhibited excellent catalytic selectivity for cellulose conversion, achieving an impressive CO yield of 35 μmol·g⁻¹·h⁻¹ and 100% selectivity. The mono-, di-, and ternary metal sulfides, which consist of only a few metal elements, lack the broad compositional tunability exhibited by (NiCdCuFeCo)_x, which contains multiple metal elements. Figure 11E shows that (NiCdCuFeCo)_x remains well stabilized under different pH values and anionic environments. Further, a mechanism diagram as in Figure 11F is proposed, in which peroxydisulfate (PDS) is excited by the (NiCdCuFeCo)_x material to generate a high concentration of single-linear O₂ and superoxide radicals, and then goes for cellulose realization decarboxylation to form CO gas. In 2023, Xu *et al.* prepared (CdZnCuCoFe)_x HEPs also by solvothermal method^[90]. As shown in Figure 11G, (CdZnCuCoFe)_x has the highest yield (achieving a high CO yield of 1.73 mmol·g⁻¹·h⁻¹) and the highest selectivity (up to 99.1%) for CO production from the decomposition of polysaccharides (guar gum) as compared to other metal sulfides. Further, introducing other peroxides [hydrogen peroxide, peroxyacetic acid, peroxymonosulfate (PMS)], it can be seen from Figure 11H that (CdZnCuCoFe)_x still has a higher yield of CO compared with CdS and (CdCu)_x, but none of their three peroxide introductions exceeds the amount of CO generated by PDS introduction. As shown in the mechanism diagrams of Figure 11I and J, Fe, Cu, and Co act as charge-rich active sites contributing electrons to reduce PDS to [•]OH, [•]SO₄⁻ and [•]O₂⁻. On the other hand, Cd and Zn act as electron-deficient active sites to oxidize PDS to ¹O₂. (CdZnCuCoFe)_x continuously converts PDS to reactive groups as electrons are gained and lost along the atomic chain. At the same time, light and heat synergistically accelerate the use of more reactive groups for attacking the biomass to efficiently convert it to CO.

Table 3. Different HEPs for CO₂ reduction

HEPs	Application	Condition	Performance	Ref.
TiZrNbHfTaO ₁₁	CO ₂ reduction	High-pressure Hg light source (Sen Lights Corporation, HL400BH-8, 400 W)	CO production (4.64 ± 0.30 μmol·g ⁻¹ ·h ⁻¹)	[78]
TiZrNbHfTaO ₁₁	CO ₂ reduction	High-pressure mercury light source (500 mW·cm ⁻²)	CO production (50 μmol·g ⁻¹ ·h ⁻¹), CH ₄ production (200 μmol·g ⁻¹ ·h ⁻¹)	[81]
Cu-(Ga _{0.2} Cr _{0.2} Mn _{0.2} Ni _{0.2} Zn _{0.2}) ₃ O ₄	CO ₂ reduction	300 W xenon lamp (PLS-SXE 300C, Beijing Bofeilai Technologies Co., Ltd.)	CO production (5.66 μmol·g _{cat} ⁻¹ ·h ⁻¹), CH ₄ production (33.84 μmol·g _{cat} ⁻¹ ·h ⁻¹)	[82]
High entropy (Ti, Hf, Nb, Ta, Mo) N nanofibers	CO ₂ reduction	300 W Xe lamp	CO production (469.0 μmol·g ⁻¹ ·h ⁻¹), CH ₄ production (242.5 μmol·g ⁻¹ ·h ⁻¹)	[83]
(NiCuMnCoZnFe) ₃ O ₄	CO ₂ reduction	300W Xe lamp (320-2,500 nm)	CO production (42.8 μmol·g ⁻¹ ·h ⁻¹), CH ₄ production (8.7 μmol·g ⁻¹ ·h ⁻¹)	[84]
TiZrNbHfTaO ₆ N ₃	CO ₂ reduction	400 W high-pressure mercury lamp (HL400BH-8 of Sen Lights Corporation) without any filtration	CO production (1.6 ± 1.5 μmol·g ⁻¹ ·h ⁻¹)	[85]
(Ga _{0.2} Cr _{0.2} Mn _{0.2} Ni _{0.2} Zn _{0.2}) ₃ O ₄	CO ₂ reduction	300 W xenon lamp (PLS-SXE 300C, Beijing Bofeilai Technologies Co., Ltd.)	CO production (23.01 μmol·g _{cat} ⁻¹ ·h ⁻¹), CH ₄ production (2.89 μmol·g _{cat} ⁻¹ ·h ⁻¹)	[86]
La(FeCoNiCrMn)O ₃	CO ₂ reduction	10 W LED light resource	CO production (527.3 μmol·g ⁻¹ ·h ⁻¹)	[87]
Ce _{0.2} Zr _{0.2} La _{0.2} Nd _{0.2} Sm _{0.2} O _{2-δ}	CO ₂ reduction	11 W UV lamp (λ = 370 nm)	-	[88]
FeCoNiCuMn HEA NPs	CO ₂ reduction	300 W Xe lamp with an AM 1.5G filter to simulate the solar light spectrum (100 mW·cm ⁻²)	CO production (235.2 μmol·g ⁻¹ ·h ⁻¹), CH ₄ production (19.9 μmol·g ⁻¹ ·h ⁻¹)	[89]

HEPs: High entropy photocatalysts; LED: light-emitting diode.

Organic transformation

HEPs offer a variety of advantages in organic conversion reactions involving the conversion of organic compounds into value-added products through a photocatalytic process. Further, the elemental diversity, adjustable elemental ratios, and structural disorder of HEPs allow researchers to tailor the photocatalyst's energy band structure, electronic properties, and surface properties to optimize its performance for a particular organic transformation reaction to facilitate the desired reaction pathway and minimize unwanted side reactions^[40,91]. HEPs can also be designed as multifunctional materials capable of performing multiple catalytic transformations simultaneously or sequentially. By integrating different catalytically active sites and functions into a single material, HEPs can facilitate complex organic synthesis pathways and simplify reaction processes. Overall, they offer significant advantages in organic transformation reactions, including enhanced catalytic activity, tunable performance, broad substrate compatibility, selective catalysis, mild reaction conditions, green and sustainable catalysis, and opportunities for functional material design. These advantages make HEPs promising candidates for advancing organic synthesis and developing new chemical transformations and methods. In 2023, Li *et al.* synthesized (CoCuZnMnNa)O_x high-entropy metal oxide nanoparticles through hydrothermal method [Figure 12A], and the mapping diagram of their sample [Figure 12B] shows that the elements of Co, Cu, Zn, Mn, Na, and O are all uniformly distributed in the sample, which can be formed in favor of the maximization of the density of the catalytically active sites, and thus the improvement of the catalytic activity^[91]. Under optimal reaction conditions, (CoCuZnMnNa)O_x achieved 88% yield and 99% selectivity for the oxidative coupling reaction of benzenethiols, with yields of over 70% for other benzenethiol derivatives [Figure 12C]. Additionally, (CoCuZnMnNa)O_x achieved 91% yield and 98% selectivity for the cyclization reaction of benzimidazoles, with yields of over 80% for other benzimidazole derivatives [Figure 12D]. Further, the mechanistic analysis of these two types of reactions is presented [Figure 12E]. (CoCuZnMnNa)O_x is photoexcited to generate photogenerated electrons and holes, and benzyl mercaptan forms a positive ion at the hole (Ar-S⁺H), which is then substituted by the electron-out-generated superoxide radical to generate a thiobenzyl radical (Ar-S[•]), and then two Ar-S[•] coupling reaction disulfide aromatizers. In the other reaction system, the N atom in the

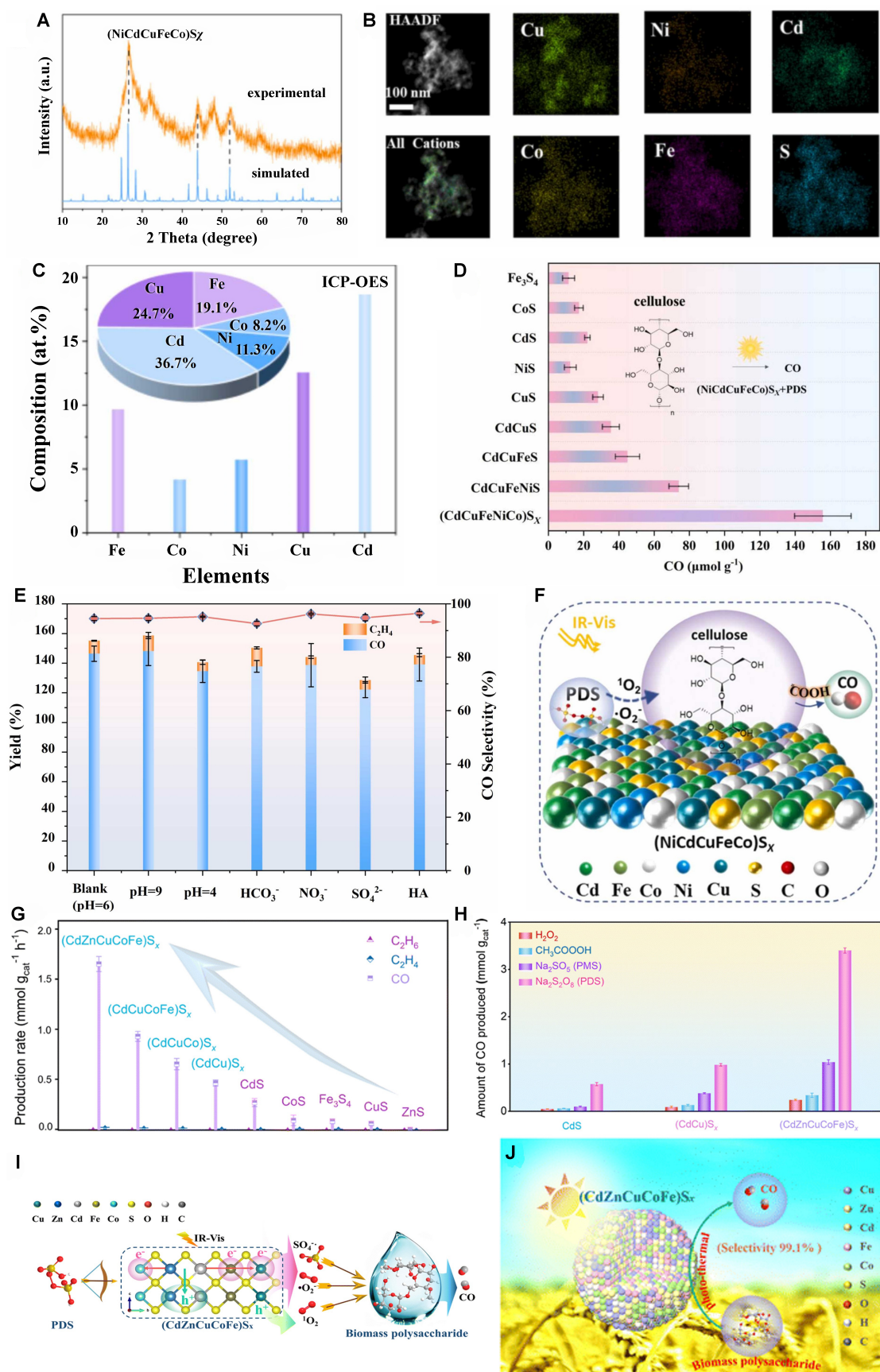


Figure 11. (A) Experimental and simulated XRD patterns of $(\text{NiCdCuFeCo})\text{S}_x$; (B) HAADF-STEM mapping image of $(\text{NiCdCuFeCo})\text{S}_x$; (C) Overall atomic percentage of metals in $(\text{NiCdCuFeCo})\text{S}_x$ as determined through ICP-OES; (D) Amount of CO produced by distinct sulfide-based catalysts; (E) Effect of ion concentration, humic acid concentration and pH on the yield and selectivity of cellulose conversion to CO; (F) The recommended reaction mechanism for the conversion of cellulose to CO via the $(\text{NiCdCuFeCo})\text{S}_x/\text{PDS}$ system. Reproduced with permission^[38]. Copyright 2024, Elsevier; (G) Amounts of CO, C_2H_4 and C_2H_6 produced over distinct sulfide-based catalysts; (H) CO generation rates in the presence of H_2O_2 , CH_3COOOH , Na_2SO_5 and $\text{Na}_2\text{S}_2\text{O}_8$, respectively; (I) Reaction mechanism for the conversion of guar gum in the $(\text{CdZnCuCoFe})\text{S}_x/\text{PDS}$ system; (J) Reaction mechanism of $(\text{CdZnCuCoFe})\text{S}_x$ nanosheets for the conversion of biomass for efficient CO generation. Reproduced with approval^[90]. Copyright 2023, Royal Society of Chemistry. XRD: X-ray diffraction; HAADF-STEM: high-angle annular dark-field scanning transmission electron microscopy; ICP-OES: inductively coupled plasma optical emission spectroscopy; PDS: peroxydisulfate.

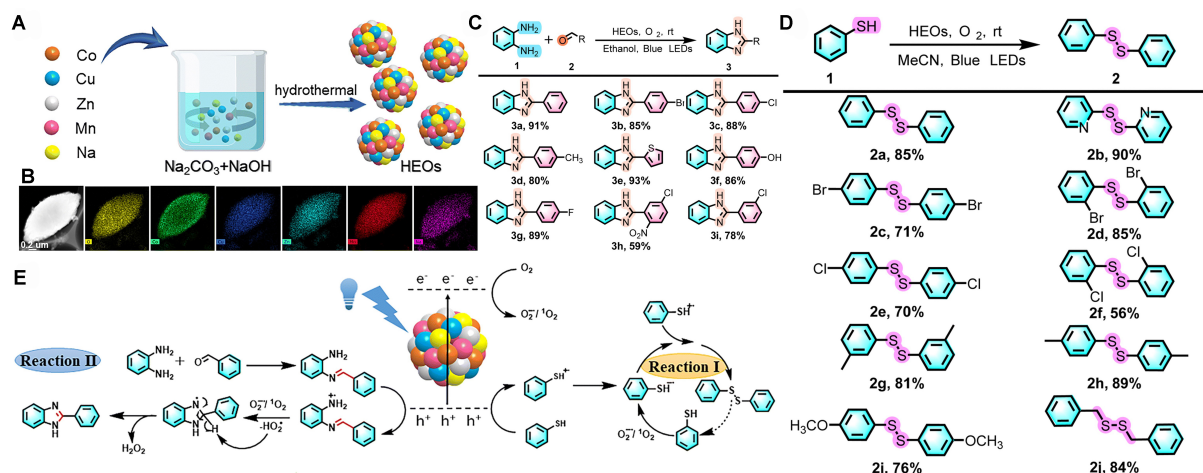


Figure 12. (A) Synthesis process of $(\text{CoCuZnMnNa})\text{O}_x$ HEOs; (B) TEM-EDX-mapping element mapping images of O, Co, Cu, Zn, Mn and Na of $(\text{CoCuZnMnNa})\text{O}_x$ HEOs; (C) $(\text{CoCuZnMnNa})\text{O}_x$ HEOs for various Photoreaction synthesis results of sulfide (C) and benzimidazole cyclization reaction product (D); (E) $(\text{CoCuZnMnNa})\text{O}_x$ HEOs for oxidative coupling of thiophenol to diphenyl disulfide and benzimidazole ring chemical reaction mechanism. procreated with approval from^[91]. Copyright 2023, Royal Society of Chemistry. HEOs: High entropy oxides; TEM: transmission electron microscopy; EDX: energy dispersive X-ray spectroscopy.

imine intermediate loses electrons to form a positive ion, which then combines with the aldehyde group on the aromatic ring to form an $\text{N}=\text{C}$ structure, and then the final product is obtained. In summary, it can be seen that HEPs have led to a significant improvement in the conversion and selectivity of specific organic reactions.

CONCLUSIONS AND OUTLOOKS

This paper presents a comprehensive analysis and summary of HEPs. The development of HEPs is presented in terms of composition, synthesis, advantages in photocatalysis, characterization methods, prediction, and energy and environmental applications. It is found that the inbuilt entropy effect and multi-component tunable constitution of HEPs play an important role in upgrading the catalytic activity and stability. Therefore, HEPs are speedily modernizing and contributing to more applications. Despite the significant advances in catalysis of HEPs, certain challenges and outlooks must be considered to noticeably optimize their functionalization for photocatalytic applications, as follows:

(1) Preparation methods. More HEPs are currently synthesized without specific morphology and crystal surface exposure, and there is an urgent need to advance rapid and versatile synthesis paths for HEPs with controllable morphology (e.g., high specific surface samples, high refractive index samples) for particular reactions. What is more, it is crucial to study the connection between structure and activity of HEPs with diverse geometries or electronic structures.

(2) High-grade characterization. Compared to conventional catalysts, there are not many characterization techniques available for the structure of HEPs (e.g., techniques for characterizing strain and interfacial effects are still in their infancy). This is not contributory to the examination of the conformational connection between electron-rich structures and catalytic active sites, as well as the veridical photocatalytic reaction mechanism.

(3) Theoretical calculations combined with ML predictions. Owing to the stochastic distribution of atoms in HEPs, creating atomic models to guide compositional combinations is a great challenge. Therefore, synthesizing HEPs with specific functions remains a great challenge. It is needed to ameliorate the related theoretical computational system and create a high-throughput database combined with ML to realize the rapid construction of HEPs. Meanwhile, the study of the reaction mechanism of HEPs in photocatalytic systems also requires modeling to reveal the reaction pathways. In short, there is an urgent need to provide more accurate simulations.

(4) Expanding the scope of application and practical application. At present, photocatalysis has not been widely used and is still in the primary stage, and the use of HEPs in photocatalysis needs more exploration, especially for some reaction systems that require efficient selectivity of target products. In addition, HEPs have a multi-component structure, which contributes to their interactive performance and wide application in the industry. Consequently, we should continue to advance the applications of HEPs and enlarge the scale of medium/large-scale experiments.

To sum up, there are a lot of exciting directions and unexplored probabilities for HEPs that need to be investigated. The development and design of multifunctional HEPs constructed for aimed catalytic reactions and other objectives are very promising. In addition, the structure, physicochemical properties, and reaction mechanisms of HEPs under complex reaction conditions require in-depth study. We believe that newer and more versatile HEPs will be developed in the future.

DECLARATIONS

Authors' contributions

Manuscript preparation: Jing, L.; Wang, H.; Roostaei, T.; Varamesh, A.; Gao, Q.

Manuscript correction: Jing, L.; Hu, J.

Availability of data and materials

Not applicable.

Financial support and sponsorship

This study was financially supported by the Natural Sciences and Engineering Research Council of Canada-Discovery Grant (10040079) (Canada).

Conflicts of interest

Hu, J. is a member of the Youth Editorial Board and is not involved in the editorial review or the decision to publish this article, while the other authors have declared that they have no conflicts of interest.

Ethical approval and consent to participate

Not applicable.

Consent for publication

Not applicable.

Copyright

© The Author(s) 2025.

REFERENCES

1. Chen, X.; Zhao, J.; Li, G.; Zhang, D.; Li, H. Recent advances in photocatalytic renewable energy production. *Energy. Mater.* **2022**, *2*, 200001. [DOI](#)
2. Ning, J.; Zhang, B.; Siqin, L.; et al. Designing advanced S-scheme CdS QDs/La-Bi₂WO₆ photocatalysts for efficient degradation of RhB. *Exploration* **2023**, *3*, 20230050. [DOI](#) [PubMed](#) [PMC](#)
3. Cao, W.; Zhang, W.; Dong, L.; et al. Progress on quantum dot photocatalysts for biomass valorization. *Exploration* **2023**, *3*, 20220169. [DOI](#) [PubMed](#) [PMC](#)
4. Rhimi, B.; Zhou, M.; Yan, Z.; Cai, X.; Jiang, Z. Cu-based materials for enhanced C₂₊ product selectivity in photo-/electro-catalytic CO₂ reduction: challenges and prospects. *Nanomicro. Lett.* **2024**, *16*, 64. [DOI](#) [PubMed](#) [PMC](#)
5. He, K.; Huang, Z.; Chen, C.; Qiu, C.; Zhong, Y. L.; Zhang, Q. Exploring the roles of single atom in hydrogen peroxide photosynthesis. *Nanomicro. Lett.* **2023**, *16*, 23. [DOI](#) [PubMed](#) [PMC](#)
6. Dhakshinamoorthy, A.; Li, Z.; Yang, S.; Garcia, H. Metal-organic framework heterojunctions for photocatalysis. *Chem. Soc. Rev.* **2024**, *53*, 3002-35. [DOI](#) [PubMed](#)
7. Dubey, A.; Sanchez, S. L.; Yang, J.; Ahmadi, M. Lead-free halide perovskites for photocatalysis via high-throughput exploration. *Chem. Mater.* **2024**, *36*, 2165-76. [DOI](#)
8. Yang, J. L.; Wang, H. J.; Qi, X.; et al. Understanding the behaviors of plasmon-induced hot carriers and their applications in photocatalysis. *ACS Appl. Mater. Interfaces.* **2024**, *16*, 12149-60. [DOI](#) [PubMed](#)
9. Liu, H.; Yan, N.; Bai, H.; Kwok, R. T. K.; Tang, B. Z. Aggregation-induced emission luminogens for augmented photosynthesis. *Exploration* **2022**, *2*, 20210053. [DOI](#) [PubMed](#) [PMC](#)
10. Sun, Z.; Zhao, H.; Yu, X.; Hu, J.; Chen, Z. Glucose photorefinery for sustainable hydrogen and value-added chemicals coproduction. *Chem. Synth.* **2024**, *4*, 4. [DOI](#)
11. Li, Y.; Zhang, D.; Qiao, W.; et al. Nanostructured heterogeneous photocatalyst materials for green synthesis of valuable chemicals. *Chem. Synth.* **2022**, *2*, 9. [DOI](#)
12. Zhang, Y.; Liu, Y.; Gong, X.; et al. Construction of piezoelectric photocatalyst Au/BiVO₄ for efficient degradation of tetracycline and studied at single-particle level. *Chem. Synth.* **2024**, *4*, 21. [DOI](#)
13. Wang, W.; Wang, X.; Gao, M.; Li, Z.; Zhou, W. Microenvironmental regulation of covalent organic frameworks for photocatalytic hydrogen peroxide production. *Coord. Chem. Rev.* **2024**, *506*, 215694. [DOI](#)
14. Gao, Z.; Ren, P.; Sun, L.; Luo, N.; Wang, F. Photocatalysts for steering charge transfer and radical reactions in biorefineries. *Nat. Synth.* **2024**, *3*, 438-51. [DOI](#)
15. Xue, J.; Fujitsuka, M.; Tachikawa, T.; Bao, J.; Majima, T. Charge trapping in semiconductor photocatalysts: a time- and space-domain perspective. *J. Am. Chem. Soc.* **2024**, *146*, 8787-99. [DOI](#) [PubMed](#)
16. Li, R.; Qiu, L. P.; Cao, S. Z.; et al. Research advances in magnetic field-assisted photocatalysis. *Adv. Funct. Mater.* **2024**, *34*, 2316725. [DOI](#)
17. Sajwan, D.; Sharma, A.; Sharma, M.; Krishnan, V. Upcycling of plastic waste using photo-, electro-, and photoelectrocatalytic approaches: a way toward circular economy. *ACS Catal.* **2024**, *14*, 4865-926. [DOI](#)
18. Wang, P.; Yang, F.; Qu, J.; et al. Recent advances and challenges in efficient selective photocatalytic CO₂ methanation. *Small* **2024**, *20*, e2400700. [DOI](#) [PubMed](#)
19. Jing, L.; Xu, Y.; Xie, M.; et al. Piezo-photocatalysts in the field of energy and environment: designs, applications, and prospects. *Nano. Energy.* **2023**, *112*, 108508. [DOI](#)
20. Zhao, H.; Liu, J.; Zhong, N.; et al. Biomass photoreforming for hydrogen and value-added chemicals co-production on hierarchically porous photocatalysts. *Adv. Energy. Mater.* **2023**, *13*, 2300257. [DOI](#)
21. Jing, L.; Xu, Y.; Xie, M.; et al. Cyano-rich g-C₃N₄ in photochemistry: design, applications, and prospects. *Small* **2024**, *20*, e2304404. [DOI](#) [PubMed](#)
22. Jing, L.; Xu, Y.; Xie, M.; et al. LnVO₄ (Ln=La, Ce, Pr, Nd, etc.)-based photocatalysts: synthesis, design, and applications. *J. Mater. Sci. Technol.* **2024**, *177*, 10-43. [DOI](#)
23. Loh, J. Y. Y.; Wang, A.; Mohan, A.; et al. Leave no photon behind: artificial intelligence in multiscale physics of photocatalyst and photoreactor design. *Adv. Sci.* **2024**, *11*, e2306604. [DOI](#) [PubMed](#) [PMC](#)
24. Qin, L.; Ma, C.; Zhang, J.; Zhou, T. Structural motifs in covalent organic frameworks for photocatalysis. *Adv. Funct. Mater.* **2024**, 2401562. [DOI](#)
25. Li, S.; Li, Y.; Huang, H. Solar-driven selective oxidation over bismuth-based semiconductors: from prolific catalysts to diverse reactions. *Adv. Funct. Mater.* **2024**, *34*, 2313883. [DOI](#)
26. Deng, C.; Wang, T.; Wu, P.; Zhu, W.; Dai, S. High entropy materials for catalysis: a critical review of fundamental concepts and applications. *Nano. Energy.* **2024**, *120*, 109153. [DOI](#)
27. Zhang, J.; Yu, Q.; Wang, Q.; et al. Strong yet ductile high entropy alloy derived nanostructured cermet. *Nano. Lett.* **2022**, *22*, 7370-7. [DOI](#) [PubMed](#)

28. Zoubi W, Putri RAK, Abukhadra MR, Ko YG. Recent experimental and theoretical advances in the design and science of high-entropy alloy nanoparticles. *Nano. Energy*. **2023**, *110*, 108362. DOI
29. Sun, L.; Wang, W.; Lu, P.; Liu, Q.; Wang, L.; Tang, H. Enhanced photocatalytic hydrogen production and simultaneous benzyl alcohol oxidation by modulating the Schottky barrier with nano high-entropy alloys. *Chinese. J. Catal.* **2023**, *51*, 90-100. DOI
30. Amiri, A.; Shahbazian-yassar, R. Recent progress of high-entropy materials for energy storage and conversion. *J. Mater. Chem. A*. **2021**, *9*, 782-823. DOI
31. Shi, Z.; Wang, L.; Huang, Y.; Kong, X. Y.; Ye, L. High-entropy catalysts: new opportunities toward excellent catalytic activities. *Mater. Chem. Front.* **2023**, *8*, 179-91. DOI
32. Xin, Y.; Li, S.; Qian, Y.; et al. High-entropy alloys as a platform for catalysis: progress, challenges, and opportunities. *ACS. Catal.* **2020**, *10*, 11280-306. DOI
33. Li, H.; Zhu, H.; Zhang, S.; Zhang, N.; Du, M.; Chai, Y. Nano high-entropy materials: synthesis strategies and catalytic applications. *Small. Struct.* **2020**, *1*, 2000033. DOI
34. Shaikh, J. S.; Rittirum, M.; Saelee, T.; et al. High entropy materials frontier and theoretical insights for logistics CO₂ reduction and hydrogenation: electrocatalysis, photocatalysis and thermo-catalysis. *J. Alloys. Compd.* **2023**, *969*, 172232. DOI
35. Gao, Y.; Liu, Y.; Yu, H.; Zou, D. High-entropy oxides for catalysis: status and perspectives. *Appl. Catal. A. Gen.* **2022**, *631*, 118478. DOI
36. Ma, J.; Huang, C. High entropy energy storage materials: synthesis and application. *J. Energy. Storage*. **2023**, *66*, 107419. DOI
37. Wu, F.; Dou, Y.; Zhou, J.; et al. High-entropy (FeCoNiCuZn)WO₄ photocatalysts-based fibrous membrane for efficient capturing and upcycling of plastic. *Chem. Eng. J.* **2023**, *470*, 144134. DOI
38. Shi, Z.; Li, C.; Huang, N.; et al. Highly selective formation of CO from domestic wastewater with Zero CO₂ emissions through solar energy catalysis. *Appl. Catal. B. Environ.* **2024**, *343*, 123542. DOI
39. Edalati, P.; Shen, X.; Watanabe, M.; et al. High-entropy oxynitride as a low-bandgap and stable photocatalyst for hydrogen production. *J. Mater. Chem. A*. **2021**, *9*, 15076-86. DOI
40. Zoubi W, Assfour B, Wahab Allaf A, Leoni S, Kang J, Ko YG. Experimental and theoretical investigation of high-entropy-alloy/support as a catalyst for reduction reactions. *J. Energy. Chem.* **2023**, *81*, 132-42. DOI
41. Badreldin, A.; Bouhali, O.; Abdel-wahab, A. Complimentary computational cues for water electrocatalysis: a DFT and ML perspective. *Adv. Funct. Mater.* **2024**, *34*, 2312425. DOI
42. Zhai, Y.; Ren, X.; Wang, B.; Liu, S. High-entropy catalyst - A novel platform for electrochemical water splitting. *Adv. Funct. Mater.* **2022**, *32*, 2207536. DOI
43. Araujo, R. B.; Edvinsson, T. Supervised AI and deep neural networks to evaluate high-entropy alloys as reduction catalysts in aqueous environments. *ACS. Catal.* **2024**, *14*, 3742-55. DOI PubMed PMC
44. Hart, G. L. W.; Mueller, T.; Toher, C.; Curtarolo, S. Machine learning for alloys. *Nat. Rev. Mater.* **2021**, *6*, 730-55. DOI
45. Katiyar, N. K.; Goel, G.; Goel, S. Emergence of machine learning in the development of high entropy alloy and their prospects in advanced engineering applications. *Emergent. Mater.* **2021**, *4*, 1635-48. DOI
46. Lu, Z.; Chen, Z. W.; Singh, C. V. Neural network-assisted development of high-entropy alloy catalysts: decoupling ligand and coordination effects. *Matter* **2020**, *3*, 1318-33. DOI
47. Yang, Z.; Gao, W. Applications of machine learning in alloy catalysts: rational selection and future development of descriptors. *Adv. Sci.* **2022**, *9*, e2106043. DOI PubMed PMC
48. Cao, L. Recent advances in the application of machine-learning algorithms to predict adsorption energies. *Trends. Chem.* **2022**, *4*, 347-60. DOI
49. Aslan, E.; Emir, Ö.; Arslan, F.; et al. Improving the optical properties of CuCoMnO_x spinel absorber using ZnO nanorod arrays for thermal collector and photocatalytic applications. *Ceram. Int.* **2024**, *50*, 9169-76. DOI
50. Gautam, A.; Das, S.; Ahmad, M. I. Band gap engineering through calcium addition in (Mg, Co, Ni, Cu, Zn)O high entropy oxide for efficient photocatalysis. *Surf. Interfaces.* **2024**, *46*, 104054. DOI
51. Zhang, Y.; Li, S.; Wang, N.; et al. Flexible amorphous (Fe_{0.5}Co_{0.5})₇₀B₂₁Ta₄Ti₅ high-entropy alloy catalyst showing high activity and stability in degrading Eosin Y. *Appl. Surf. Sci.* **2023**, *616*, 156567. DOI
52. Yu, Y.; Liu, S.; Wang, H.; et al. Design, synthesis and photocatalytic performance of A₃₂Ti₈Sn₈Nb₄Ta₄Me₈O₉₆ (A=Ba, Sr; Me=Fe, Ga) perovskite structure high entropy oxides. *J. Solid. State. Chem.* **2023**, *317*, 123694. DOI
53. Pang, Z.; Wang, B.; Yan, X.; et al. Unique Sillén-structured multimetal high entropy oxyhalide Pb_xCd_{1-x}BiO₂Br with enhanced photocatalytic activity. *Appl. Surf. Sci.* **2022**, *578*, 151921. DOI
54. Gul, A.; Ullah, R.; Sun, J.; Munir, T.; Bai, S. Synthesis of mesoporous TiO₂/BMMs via hydrothermal method and its potential application toward adsorption and photocatalytic degradation of crystal violet from aqueous solution. *Arab. J. Chem.* **2022**, *15*, 103530. DOI
55. Du, M.; Liu, S.; Ge, Y.; et al. Preparation and effect of grain size on the thermal stability, phase transition, mechanical property, and photocatalytic property of pyrochlore (La_{0.2}Nd_{0.2}Sm_{0.2}Gd_{0.2}Y_{0.2})₂Zr₂O₇ high-entropy oxide. *Ceram. Int.* **2022**, *48*, 20667-74. DOI
56. Liu, S.; Du, M.; Ge, Y.; et al. Enhancement of high entropy oxide (La_{0.2}Nd_{0.2}Sm_{0.2}Gd_{0.2}Y_{0.2})₂Zr₂O₇ mechanical and photocatalytic properties via Eu doping. *J. Mater. Sci.* **2022**, *57*, 7863-76. DOI
57. Wang, T.; Wang, Y.; Wang, N.; Xu, S.; Han, Z.; Wang, Y. Development of a novel (Ni₄₀Fe₃₀Co₂₀Al₁₀)₉₀Ti₁₀ high-entropy alloy with excellent photocatalytic performance. *Mater. Lett.* **2021**, *283*, 128817. DOI

58. Fu, H.; Li, S.; Lin, Y.; et al. Enhancement of piezo–photocatalytic activity in perovskite ($\text{Bi}_{0.2}\text{Na}_{0.2}\text{Ba}_{0.2}\text{K}_{0.2}\text{La}_{0.2}$) TiO_3 oxides via high entropy induced lattice distortion and energy band reconfiguration. *Ceram. Int.* **2024**, *50*, 9159–68. DOI
59. Jia, D.; Chigan, T.; Li, X.; Li, H.; Yang, P. Photocatalytic degradation performance for high-entropy oxide ($\text{La}_{0.2}\text{Ce}_{0.2}\text{Gd}_{0.2}\text{Zr}_{0.2}\text{Fe}_x$) O_2 enriched with defects. *J. Alloys. Compd.* **2024**, *982*, 173808. DOI
60. Das, S.; Sanjay, M.; Singh, G. A. R.; Behera, R.; Tiwary, C. S.; Chowdhury, S. Low bandgap high entropy alloy for visible light-assisted photocatalytic degradation of pharmaceutically active compounds: performance assessment and mechanistic insights. *J. Environ. Manage.* **2023**, *342*, 118081. DOI PubMed
61. Das, S.; Sanjay, M.; Kumar, S.; Sarkar, S.; Tiwary, C. S.; Chowdhury, S. Magnetically separable MnFeCoNiCu-based high entropy alloy nanoparticles for photocatalytic oxidation of antibiotic cocktails in different aqueous matrices. *Chem. Eng. J.* **2023**, *476*, 146719. DOI
62. He, L.; Zhou, J.; Sun, Y.; Liu, D.; Liu, X. Efficient removal of tetracycline hydrochloride by high entropy oxides in visible photo-Fenton catalytic process. *Environ. Technol.* **2023**, 1–14. DOI
63. Chang, S. C.; Chen, H.; Chen, P.; Lee, J.; Wu, J. M. Piezo-photocatalysts based on a ferroelectric high-entropy oxide. *Appl. Catal. B. Environ.* **2023**, *324*, 122204. DOI
64. Yu, X.; Wang, S.; Zhang, Y.; et al. Novel high entropy alloy/ NiAl_2O_4 photocatalysts for the degradation of tetracycline hydrochloride: Heterojunction construction, performance evaluation and mechanistic insights. *Ceram. Int.* **2024**, *50*, 29528–46. DOI
65. Zakir, O.; Guler, O.; Idouhli, R.; et al. Enhanced photocatalytic abilities of innovative NbTaZrMoW high-entropy alloys (HEAs): a comparative analysis with its high entropy oxide (HEO) counterpart. *J. Mater. Sci.* **2024**, *59*, 12050–64. DOI
66. Das, S.; Kumar, S.; Sarkar, S.; Pradhan, D.; Tiwary, C. S.; Chowdhury, S. High entropy spinel oxide nanoparticles for visible light-assisted photocatalytic degradation of binary mixture of antibiotic pollutants in different water matrixes. *J. Mater. Chem. A.* **2024**, *12*, 16815–30. DOI
67. Wen, N.; Mu, X.; Zhu, Y.; et al. Preparation of novel layered high entropy bismuth-based materials and their photocatalytic degradation mechanism. *Langmuir* **2024**, *40*, 9020–7. DOI PubMed
68. Jiang, X.; Liu, L.; Liu, Y.; Wang, Y.; Hou, Z. Molten salt synthesis of A-site disordered niobate microcrystals with tetragonal tungsten bronze structure. *J. Cryst. Growth.* **2024**, *627*, 127493. DOI
69. Zhang, F.; Zhou, W.; Zhang, Y.; et al. Spectroscopic analyses and photocatalytic properties of transition group metal oxide films with different entropy values. *Mat. Sci. Semicon. Proc.* **2024**, *169*, 107928. DOI
70. Nundy, S.; Tatar, D.; Kojčinović, J.; et al. Bandgap engineering in novel fluorite-type rare earth high-entropy oxides (RE-HEOs) with computational and experimental validation for photocatalytic water splitting applications. *Adv. Sustain. Syst.* **2022**, *6*, 2200067. DOI
71. Wu, P. Y.; Le, K. T.; Lin, H. Y.; Chen, Y. C.; Wu, P. H.; Wu, J. M. Flexoelectric catalysts based on hierarchical wrinkling surface of centrosymmetric high-entropy oxide. *ACS. Nano.* **2023**, *17*, 17417–26. DOI PubMed
72. Zhong, Z.; Fu, H.; Wang, S.; et al. A universal synthesis strategy for lanthanide sulfide nanocrystals with efficient photocatalytic hydrogen production. *Small* **2023**, *19*, e2301392. DOI PubMed
73. Guo, H.; Wang, G.; Li, H.; Xia, C.; Dong, B.; Cao, L. Direct Z-scheme high-entropy metal phosphides/ ZnIn_2S_4 heterojunction for efficient photocatalytic hydrogen evolution. *Colloid. Surface. A.* **2023**, *674*, 131915. DOI
74. Cai, L.; Yan, B.; Shi, H.; Liu, P.; Yang, G. A Medium-entropy oxide as a promising cocatalyst to promote photocatalytic hydrogen evolution. *J. Colloid. Interface. Sci.* **2023**, *646*, 625–32. DOI PubMed
75. Edalati, P.; Wang, Q.; Razavi-khosroshahi, H.; Fuji, M.; Ishihara, T.; Edalati, K. Photocatalytic hydrogen evolution on a high-entropy oxide. *J. Mater. Chem. A.* **2020**, *8*, 3814–21. DOI
76. Qi, S.; Zhu, K.; Xu, T.; et al. Water-stable high-entropy metal-organic framework nanosheets for photocatalytic hydrogen production. *Adv. Mater.* **2024**, *36*, e2403328. DOI PubMed
77. Edalati, P.; Itagoe, Y.; Ishihara, H.; et al. Visible-light photocatalytic oxygen production on a high-entropy oxide by multiple-heterojunction introduction. *J. Photoch. Photobio. A.* **2022**, *433*, 114167. DOI
78. Akrami, S.; Murakami, Y.; Watanabe, M.; et al. Defective high-entropy oxide photocatalyst with high activity for CO_2 conversion. *Appl. Catal. B. Environ.* **2022**, *303*, 120896. DOI
79. Ling, H.; Sun, M.; Han, H.; et al. High-entropy lithium niobate nanocubes for photocatalytic water splitting under visible light. *J. Phys. Chem. Lett.* **2024**, *15*, 5103–11. DOI PubMed
80. Güler, Ö.; Boyrazlı, M.; Albayrak, M. G.; Güler, S. H.; Ishihara, T.; Edalati, K. Photocatalytic hydrogen evolution of TiZrNbHfTaO_x high-entropy oxide synthesized by mechano-thermal method. *Materials* **2024**, *17*, 853. DOI PubMed PMC
81. Pourmand, T. Z.; Fromme, T.; Reichenberger, S.; et al. Laser fragmentation of a high-entropy oxide for enhanced photocatalytic carbon dioxide (CO_2) conversion and hydrogen (H_2) production. *Adv. Powder. Technol.* **2024**, *35*, 104448. DOI
82. Zhang, Y.; Jiang, Z.; Zhang, R.; Wang, K.; Wang, X. Cu-($\text{Ga}_{0.2}\text{Cr}_{0.2}\text{Mn}_{0.2}\text{Ni}_{0.2}\text{Zn}_{0.2}$) O_4 heterojunction derived from high entropy oxide precursor and its photocatalytic activity for CO_2 reduction with water vapor. *Appl. Surf. Sci.* **2024**, *651*, 159226. DOI
83. Li, W.; Sun, Y.; Ye, L.; et al. Preparation of high entropy nitride ceramic nanofibers from liquid precursor for CO_2 photocatalytic reduction. *J. Am. Ceram. Soc.* **2022**, *105*, 3729–34. DOI
84. Zhang, L.; Xia, S.; Zhang, X.; et al. Low-temperature synthesis of mesoporous half-metallic high-entropy spinel oxide nanofibers for photocatalytic CO_2 reduction. *ACS. Nano.* **2024**, *18*, 5322–34. DOI PubMed
85. Akrami, S.; Edalati, P.; Shundo, Y.; et al. Significant CO_2 photoreduction on a high-entropy oxynitride. *Chem. Eng. J.* **2022**, *449*, 137800. DOI

86. Jiang, Z.; Zhang, R.; Zhao, H.; et al. Preparation of $(\text{Ga}_{0.2}\text{Cr}_{0.2}\text{Mn}_{0.2}\text{Ni}_{0.2}\text{Zn}_{0.2})_3\text{O}_4$ high-entropy oxide with narrow bandgap for photocatalytic CO_2 reduction with water vapor. *Appl. Surf. Sci.* **2023**, *612*, 155809. DOI
87. Wang, M.; Li, L.; Li, Y.; et al. Entropy engineering of La-based perovskite for simultaneous photocatalytic CO_2 reduction and biomass oxidation. *Chem. Commun.* **2023**, *59*, 14673-6. DOI PubMed
88. Tatar, D.; Ullah, H.; Yadav, M.; et al. High-entropy oxides: a new frontier in photocatalytic CO_2 hydrogenation. *ACS. Appl. Mater. Interfaces.* **2024**, *16*, 29946-62. DOI PubMed
89. Huang, H.; Zhao, J.; Guo, H.; et al. Noble-metal-free high-entropy alloy nanoparticles for efficient solar-driven photocatalytic CO_2 reduction. *Adv. Mater.* **2024**, *36*, e2313209. DOI PubMed
90. Xu, Y.; Wang, L.; Shi, Z.; et al. Peroxide-mediated selective conversion of biomass polysaccharides over high entropy sulfides via solar energy catalysis. *Energy. Environ. Sci.* **2023**, *16*, 1531-9. DOI
91. Li, M.; Mei, S.; Zheng, Y.; Wang, L.; Ye, L. High-entropy oxides as photocatalysts for organic conversion. *Chem. Commun.* **2023**, *59*, 13478-81. DOI PubMed

**Liquan Jing**

Liquan Jing received his Ph.D. in Environmental Science and Engineering from Jiangsu University in 2021. He is currently a postdoctoral researcher in the Department of Chemical and Petroleum Engineering at the University of Calgary under the guidance of Prof. Jinguang Hu. His current research mainly focuses on the design and synthesis of functional photocatalysts for sustainable hydrogen, conversion of biomass into other high value-added biological products, and methane conversion.

**Hui Wang**

Hui Wang is a Ph.D. student at the University of Calgary under the supervision of Prof. Jinguang Hu. She obtained her Master's degree from Tianjin University of Science and Technology in 2021. Her current research focuses on lignocellulosic biomass conversion in photocatalysis.

**Tayebbeh Roostaei**

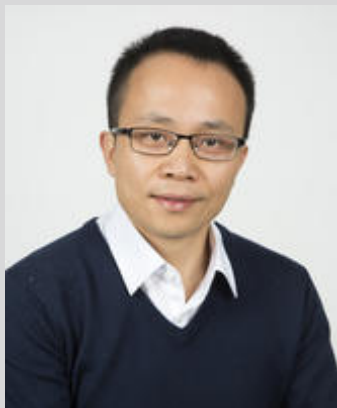
Tayebbeh Roostaei earned her Ph.D. in Chemical Engineering from Shiraz University in Iran, focusing on producing syngas through the dry reforming of methane using various catalysts. During her doctoral studies, she spent over a year as a visiting student at the University of Calgary, collaborating with Dr. Jinguang Hu's research group. There, she worked on hydrogen production via photocatalysis and published several significant papers in this field. Tayebbeh possesses extensive hands-on experience in synthesizing catalysts and operating both batch and continuous reactors. She is currently a Postdoctoral Associate at the University of Calgary, where her research is dedicated to advancing bio-oil upgrading processes to contribute to sustainable energy solutions.

**Amir Varamesh**

Amir Varamesh is a Ph.D. candidate in Environmental Engineering at the University of Calgary. He obtained his B.Sc. and M.Sc. degrees in Petroleum Engineering from Amirkabir University of Technology and the University of Tehran, respectively. Amir has published peer-reviewed articles in high-impact journals such as *Chemical Engineering Journal*, *Renewable and Sustainable Energy Reviews*, and *Journal of Hazardous Materials*. He has also received several national and international scholarships and awards. With a strong background in the development and application of sustainable biobased materials, Amir's research focuses on advancing energy and environmental solutions.

**Qi Gao**

Qi Gao is pursuing a Ph.D. degree in the Chinese Academy of Forestry. He is currently a visiting student in the Department of Chemical and Petroleum Engineering at the University of Calgary under the guidance of Prof. Jinguang Hu. His current research mainly focuses on the conversion of biomass into other high value-added biological products.

**Jinguang Hu**

Jinguang Hu received his Ph.D from The University of British Columbia (UBC) in 2014 and subsequently conducted postdoctoral research in the UBC BioProducts Institute (Canada) and Aalto-VTT HYBER Center (Academy of Finland's Centre of Excellence in Molecular Engineering of Biosynthetic Hybrid Materials research). He is currently an Assistant Professor in the Department of Chemical and Petroleum Engineering at the University of Calgary. His research, supported by the Canada First Research Excellence Fund (CFREF) Initiative, centers on utilizing photo/bio-catalysts to design and fabricate bioinspired materials or systems for Energy, Environmental, and Medical applications.